

# 1 Locally misfolded HER2 expressed on cancer cells is a promising target for development of 2 cancer-specific antibodies

3  
4 Takao Arimori<sup>1,6,\*</sup>, Emiko Mihara<sup>1</sup>, Hiroyuki Suzuki<sup>2,3</sup>, Tomokazu Ohishi<sup>4,5</sup>, Tomohiro Tanaka<sup>2</sup>, Mika  
5 K. Kaneko<sup>2,3</sup>, Junichi Takagi<sup>1</sup>, Yukinari Kato<sup>2,3,\*</sup>

6  
7 <sup>1</sup>Institute for Protein Research, Osaka University, 3-2. Yamadaoka, Suita, Osaka 565-0871, Japan

8 <sup>2</sup>Department of Molecular Pharmacology, Tohoku University Graduate School of Medicine, 2-1,  
9 Seiryomachi, Aoba-ku, Sendai, Miyagi 980-8575, Japan

10 <sup>3</sup>Department of Antibody Drug Development, Tohoku University Graduate School of Medicine, 2-1,  
11 Seiryomachi, Aoba-ku, Sendai, Miyagi 980-8575, Japan

12 <sup>4</sup>Institute of Microbial Chemistry (BIKAKEN), Numazu, Microbial Chemistry Research Foundation,  
13 18-24, Miyamoto, Numazu-shi, Shizuoka 410-0301, Japan

14 <sup>5</sup>Institute of Microbial Chemistry (BIKAKEN), Laboratory of Oncology, Microbial Chemistry  
15 Research Foundation, 3-14-23, Kamiosaki, Shinagawa-ku, Tokyo 141-0021, Japan

16 <sup>6</sup>Lead contact

17 \*Correspondence: arimori@protein.osaka-u.ac.jp (T.A.), yukinari.kato.e6@tohoku.ac.jp (Y. K.)

## 18 19 20 **Summary**

21 Overexpression of human epidermal growth factor receptor 2 (HER2) in breast and gastric  
22 cancers is known to be associated with poor prognosis, making it an attractive therapeutic target. Here,  
23 we established a novel cancer-specific anti-HER2 antibody, H<sub>2</sub>Mab-214. H<sub>2</sub>Mab-214 reacted with  
24 HER2 on cancer cells, but unlike the therapeutic antibody trastuzumab, did not react with HER2 on  
25 normal cells in flow cytometry. Using X-ray crystallography, we revealed that H<sub>2</sub>Mab-214 recognizes  
26 a structurally disrupted portion in the HER2 domain IV, which normally forms a  $\beta$ -sheet. This  
27 misfolding was shown to be inducible by site-directed mutagenesis mimicking the disulfide bond  
28 defects that may occur in cancer cells, indicating that the local misfolding in the Cys-rich domain IV  
29 governs the cancer-specificity of H<sub>2</sub>Mab-214. Furthermore, we showed that H<sub>2</sub>Mab-214 effectively  
30 suppresses tumor growth in xenograft mouse models. Our findings offer a potential strategy for  
31 developing cancer-specific therapeutic antibodies that target partially misfolded cell surface receptors.

## 32 33 **Introduction**

34 Human epidermal growth factor receptor (HER) family of receptor tyrosine kinases consists of  
35 four members: EGFR (HER1), HER2, HER3, and HER4. They play important roles in regulating cell  
36 proliferation, differentiation, and migration, while being implicated in many cancers. More than ten

37 ligands for HER members have been identified, including epidermal growth factor, transforming  
38 growth factor alpha, and neuregulins (NRGs) 1-4, yet HER2 has no known direct activating ligand.<sup>1</sup>  
39 The extracellular region of all HER family members is commonly composed of four domains (I-IV).  
40 In the absence of ligands, those receptors other than HER2 are stabilized in an inactive “tethered”  
41 conformation where a protruding loop (also called dimerization arm) in the domain II interacts with  
42 the domain IV.<sup>2-4</sup> Upon ligand binding, the receptors undergo a large conformational change from  
43 “tethered” to “extended” and form homo- or heterodimers via the dimerization arm, resulting in the  
44 autophosphorylation of the cytoplasmic tyrosine kinase domain.<sup>5-7</sup> HER2 is unique in that it always  
45 adopts extended conformation even in the monomeric state.<sup>8</sup> It has recently been shown that the  
46 structure of HER2 forming a heterodimer with HER3 is very similar to that of the monomeric state.<sup>9</sup>  
47 Hence, HER2 is always ready to be dimerized at cell surface, making it a preferable dimerization  
48 partner for other HER family members.<sup>10</sup> In addition, overexpression of HER2 promotes the formation  
49 of HER2 homodimers, leading to ligand-independent signaling.<sup>11</sup> HER2 overexpression is found in  
50 ~20% of breast cancers and is associated with poor prognosis, higher rates of recurrence, and shorter  
51 overall survival.<sup>12</sup> HER2 overexpression is also observed in ~20% of gastric cancers.<sup>13</sup>

52 Trastuzumab, a monoclonal antibody (mAb) against HER2, recognizes the domain IV<sup>8</sup> and  
53 exhibits an anti-proliferating effect *in vitro* and a potent antitumor effect *in vivo*.<sup>14</sup> The addition of  
54 trastuzumab treatment to a standard chemotherapy improves objective response rates, progression-free  
55 survival, and overall survival in HER2-positive breast cancer patients with metastasis.<sup>15</sup> Trastuzumab  
56 has been the standard treatment for HER2-positive breast cancers<sup>16</sup> and HER2-positive gastric  
57 cancers.<sup>17</sup> Clinically, the efficacy of trastuzumab involves immunologic engagement.<sup>14</sup> The Fc domain  
58 of trastuzumab mediates the engagement with Fc $\gamma$  receptors (Fc $\gamma$ Rs) on various immune cells.  
59 Trastuzumab-Fc $\gamma$ R binding allows for phagocytosis of antibody-bound tumor cells, which is called  
60 antibody-dependent cellular phagocytosis. The Fc $\gamma$ R engagement also activates macrophages,  
61 dendritic cells, and neutrophils, which can change adaptive immune responses through chemotaxis,  
62 cytokine production, and antigen presentation. Furthermore, the Fc $\gamma$ R engagement mediates the  
63 activation of natural killer (NK) cells which attack and lyse the target tumor cells, termed antibody-  
64 dependent cellular cytotoxicity (ADCC).<sup>18</sup> Margetuximab was developed by introducing several  
65 mutations in trastuzumab to improve the Fc $\gamma$ RIIIA engagement (and thus ADCC activity),<sup>19</sup> and was  
66 approved by U.S. Food and Drug Administration (FDA) and showed significant improvement in  
67 progression-free survival in heavily pretreated patients.<sup>20,21</sup> In addition to ADCC, the Fc domain of  
68 those mAbs can exert complement-dependent cytotoxicity (CDC).<sup>22,23</sup>

69 Although trastuzumab exhibits potent antitumor effect, some patients develop resistance against  
70 trastuzumab treatment, which can be attributed to the hyperactivation caused by the heterodimerization  
71 with HER3.<sup>24</sup> Pertuzumab, another clinically approved HER2-targeting mAb, recognizes the domain  
72 II and prevents NRG1-induced heterodimerization with HER3 and intracellular signaling.<sup>25</sup> Thus,

73 pertuzumab is considered to have a complementary mechanism of trastuzumab,<sup>26</sup> and the double anti-  
74 HER2 blockade has become the standard therapy in the initial management of metastatic HER2-  
75 positive breast cancer.<sup>15</sup> Furthermore, combination therapy using trastuzumab, pertuzumab, and  
76 chemotherapy has been evaluated and found to show even higher clinical benefit.<sup>27</sup>

77 Despite the proven success of HER2-targeted immunotherapies described above, they still suffer  
78 from several adverse effects, including cardiotoxicity.<sup>28</sup> Because of this side effect, routine cardiac  
79 monitoring is required in clinic during the anti-HER2 antibody treatment.<sup>28</sup> Interestingly, mice lacking  
80 *ErbB2* (ortholog of HER2) display embryonic lethality due to the dysfunctions associated with a lack  
81 of cardiac trabeculae,<sup>29</sup> and ventricular-restricted *ErbB2* deficiency in mice shows features of dilated  
82 cardiomyopathy.<sup>30</sup> These results indicate that HER2 plays important role(s) in normal heart  
83 development and homeostasis. As a proteomic study of healthy human tissues revealed a high level of  
84 broad expression of HER2,<sup>31</sup> anti-HER2 mAb therapies may attack normal tissues not limited to the  
85 heart, which may lead to other side effects including ones that are not clearly recognized at present.  
86 Therefore, it is highly desirable to use anti-HER2 mAbs that can exclusively recognize HER2  
87 expressed on cancer cells, although such reagents have not been available to this day.

88 In this study, we succeeded in establishing a novel mAb highly specific against HER2 expressed  
89 on cancer cells but not on normal cells. This antibody, H<sub>2</sub>Mab-214, was established through standard  
90 immunization and hybridoma technology, but incorporating a special screening strategy called cancer-  
91 specific mAb or CasMab method we have developed previously.<sup>32-35</sup> The cancer-specificity of H<sub>2</sub>Mab-  
92 214 was extensively investigated by flow cytometry analysis using various cell lines of normal or  
93 cancer origins, and its antitumor potential was confirmed by *in vivo* xenograft model. Most importantly,  
94 we clarified the molecular basis of H<sub>2</sub>Mab-214's cancer specificity by determining the crystal structure  
95 of its complex with HER2-derived peptide. Combined with the structure-guided mutagenesis at the  
96 epitope region, we show evidence that the local misfolding of HER2 domain IV Cys-rich region  
97 governs the cancer-specificity of H<sub>2</sub>Mab-214, pointing toward a new way of searching cancer-specific  
98 antibodies against various cell surface receptors.

99

## 100 **Results**

### 101 ***Cancer-specific HER2 recognition by H<sub>2</sub>Mab-214.***

102 We have previously established a mouse anti-HER2 mAb H<sub>2</sub>Mab-119 (IgG<sub>1</sub>, kappa) by  
103 immunizing mice with HER2 ectodomain (HER2ec) produced in glioblastoma LN229 cells.<sup>36</sup> This  
104 antibody is judged as a pan-HER2 mAb that reacts with HER2 regardless of the cell type, because its  
105 FACS staining pattern is indistinguishable from that of trastuzumab (Figures 1A and 1B). In flow  
106 cytometric analysis using saturating concentrations of each antibody, H<sub>2</sub>Mab-119 and trastuzumab  
107 brightly stained CHO-K1 cells expressing exogenously introduced HER2 (CHO/HER2) (Figure 1A)  
108 as well as BT-474 and SK-BR-3 breast cancer cell lines that are known to express endogenous HER2

109 (Figure 1B).<sup>37</sup> They also recognized immortalized normal cell lines, including HEK293T (embryonic  
110 kidney), HaCaT (keratinocyte), and MCF 10A (mammary gland epithelial cell), but not triple-negative  
111 breast cancer (TNBC) cell line, MDA-MB-468 cells known to be HER2-negative (Figure 1B).<sup>38</sup>

112 Next we aimed at obtaining anti-HER2 mAbs that recognize HER2 only when expressed on  
113 cancer cells. We incorporated differential screening protocol in the hybridoma selection step<sup>32</sup> and  
114 succeeded in establishing a few mAbs that recognized HER2-positive cancer cell lines, but not HER2-  
115 expressing normal cells. As shown in Figure 1B, one of the clones, H<sub>2</sub>Mab-214 (IgG<sub>1</sub>, kappa), reacted  
116 with BT-474 and SK-BR-3 cells, but not with HEK293T, HaCaT, and MCF 10A cells. H<sub>2</sub>Mab-214  
117 also recognized CHO/HER2 (Figure 1A), but the reactivity was relatively low compared to that of  
118 trastuzumab and H<sub>2</sub>Mab-119. These results suggest that H<sub>2</sub>Mab-214 exhibits specificity to HER2-  
119 positive breast cancer cells.

120

#### 121 ***Epitope mapping of H<sub>2</sub>Mab-214.***

122 Puzzled by the apparent cancer cell specificity of H<sub>2</sub>Mab-214 in its HER2 recognition, we next  
123 explored its binding epitope. To this end, we generated a series of N-terminal deletion mutants of  
124 HER2 by successively removing domain I ( $\Delta$ N218), domain II ( $\Delta$ N342), and domain III ( $\Delta$ N511)  
125 (Figure 2A). The comparable expression levels of these mutants on CHO-K1 cells were confirmed by  
126 the staining with NZ-1 antibody against the 16-residue PA tag attached to the N-terminus of the  
127 truncation mutants. H<sub>2</sub>Mab-214 exhibited full reactivity toward all mutants (Figure 2B), indicating  
128 that its epitope lies exclusively within the domain IV. In contrast, the reactivity of H<sub>2</sub>Mab-119 was  
129 completely lost upon the deletion of the domain I alone, suggesting the critical involvement of domain  
130 I in its HER2 recognition. To narrow down further the location of H<sub>2</sub>Mab-214 epitope, we synthesized  
131 overlapping 20-mer peptides covering the domain IV and tested their reactivity by ELISA. As shown  
132 in Figure 2C, H<sub>2</sub>Mab-214 showed strong reactivity with the peptide corresponding to residues 603-  
133 622. Subsequent analysis using the second set of shorter peptides derived from this region revealed  
134 that the linear segment Pro612-Asp618 of HER2 confers the minimally required binding epitope for  
135 H<sub>2</sub>Mab-214 (Figure 2D). Finally, binding toward alanine-substituted HER2 peptides were evaluated  
136 to see the contribution of individual amino acid. H<sub>2</sub>Mab-214 showed significantly reduced reactivity  
137 toward K615A and F616A peptides, indicating that Lys615 and Phe616 have major contribution to  
138 the recognition by H<sub>2</sub>Mab-214 (Figure 2E).

139

#### 140 ***Crystallographic analysis of H<sub>2</sub>Mab-214 in complex with the epitope peptide.***

141 The epitope mapping of H<sub>2</sub>Mab-214 revealed that it recognized linear 7-residue peptide <sub>612-</sub>  
142 PIWKFPD-<sub>618</sub>. This segment and the regions surrounding it are present in all major variants of HER2,  
143 and they do not contain sequence motifs suspected to undergo chemical modifications including  
144 glycosylation, phosphorylation, and deamidation (Figure S1A). Also, this segment is partially

145 overlapped with the binding footprint of pan-HER2 reactive trastuzumab (residues 579-625) (Figure  
146 S1).<sup>9</sup> Therefore, it is difficult to explain the cancer specificity of H<sub>2</sub>Mab-214 simply by cancer-specific  
147 chemical alterations or large domain-wise conformational change to expose its epitope. To understand  
148 how H<sub>2</sub>Mab-214 distinguishes HER2 expressed on cancer cells from that on normal cells, we  
149 performed a crystallographic analysis of H<sub>2</sub>Mab-214 in complex with its epitope peptide. To this end,  
150 antigen-binding domain of H<sub>2</sub>Mab-214 was expressed as a small and hyper-crystallizable antibody  
151 fragment, F<sub>v</sub>-clasp,<sup>39</sup> and crystallized in the presence of the excess amount of HER2 (611-618) peptide,  
152 and the complex structure was solved at 1.75-Å resolution (Table S1, Figure S2A). At the antigen  
153 binding site of H<sub>2</sub>Mab-214, a clear electron density corresponding to the epitope peptide was observed,  
154 allowing us to build models for all eight residues of the peptide (Figure S2B). The bound peptide is in  
155 a compact U-shaped conformation (Figure 3A), but unlike the typical turn conformation found in  
156 protein loops, it is not maintained via intramolecular main chain hydrogen bonds. Rather, the  
157 conformation is stabilized by intermolecular hydrogen bonding interactions formed between the  
158 residues from the peptide and Gly31B (CDR-H1), Arg58, Arg95 (CDR-H3), Ala98 (CDR-H3), and  
159 Trp100A (CDR-H3) of H<sub>2</sub>Mab-214 (Figure 3B). In addition, numerous inter- and intramolecular van  
160 der Waals contacts formed throughout the peptide reinforce highly complementary recognition  
161 interface that warrant high affinity for such a short stretch of amino acids (Figure 3A). Among the  
162 peptide residues, Lys615 and Phe616 appear to form particularly important interactions: the side chain  
163 of Lys615 forms salt bridges with two aspartic acid residues (Asp54 and Asp56) in CDR-H2 (Figure  
164 3B), while the side chain of Phe616 is inserted into a deep pocket at the center of the antigen binding  
165 site and in contact with the surrounding residues (Figure 3A). These observations are in good  
166 agreement with the results of the alanine scanning (Figure 2E).

167 We also conducted a crystallographic analysis for the pan-HER2 antibody H<sub>2</sub>Mab-119. As  
168 H<sub>2</sub>Mab-119 was found to retain high binding affinity for the HER2 domain I fragment (Figure S2C),  
169 the H<sub>2</sub>Mab-119 Fab was co-crystallized with the domain I fragment. In the complex structure solved  
170 at 1.69-Å resolution, H<sub>2</sub>Mab-119 is in contact with two β-strands and multiple loops of the domain I,  
171 indicating that H<sub>2</sub>Mab-119 recognizes three-dimensional (i.e., non-linear) epitope, which is in contrast  
172 to H<sub>2</sub>Mab-214 (Figures 3C and S2D).

173

174 ***Structural comparison of the epitope peptide bound to H<sub>2</sub>Mab-214 and the corresponding region in***  
175 ***published HER2 structures.***

176 HER2 domain IV has a stalk-like structure consisting of multiple short β-sheets stabilized by 10  
177 disulfide bonds, and the H<sub>2</sub>Mab-214 epitope sequence (Pro612 to Asp618) is located near its C-  
178 terminus (Figure 3D). So far, ten HER2 ectodomain structures containing atomic models of the  
179 Pro612-Asp618 region have been reported (i.e. PDB IDs: 1n8z, 3be1, 3n85, 6bgt, 6j71, 6oge, 7mn5,  
180 7mn6, 7mn8, and 8ffj), of which 3n85 and 6j71 are relatively well modeled with no disordered regions

181 in the domain IV. In all of these structures, the Pro612-Asp618 region assumes an extended  
182 conformation, with its central segment (Ile613 to Phe616) assuming a  $\beta$ -strand sandwiched by two  
183 strands to form a  $\beta$ -sheet (Figure 3D, inset). This "canonical" conformation of the 612-618 segment  
184 (Figure 3E) is drastically different from the U-shaped conformation seen in the same peptide bound to  
185 H<sub>2</sub>Mab-214 (Figures 3F). Analysis of the residue-wise main chain dihedral angles for the H<sub>2</sub>Mab-214-  
186 captured peptide revealed large divergence from the values obtained for the published ectodomain  
187 structures, especially at Trp614, Lys615, and Phe616 (Table 1). Such fundamental difference in the  
188 conformation tells us that the 612-618 segment needs to be dislodged or "pulled-out" from the  $\beta$ -sheet  
189 to be recognized by H<sub>2</sub>Mab-214, suggesting that the HER2 molecules reactive with H<sub>2</sub>Mab-214 must  
190 undergo local unfolding near its epitope region (Figures 3G and 3H).

191

### 192 ***Effect of forced unfolding of HER2 by DTT treatment on the reactivity of anti-HER2 mAbs.***

193 Structural studies suggested that H<sub>2</sub>Mab-214 preferentially recognizes HER2 domain IV when it  
194 is structurally compromised. To validate this hypothesis, we sought to artificially disrupt the tertiary  
195 structure of HER2 on normal cells and investigated antibody bindings to these cells. HER2 has many  
196 disulfide bonds in its extracellular region contributing to the overall structural stabilization at varying  
197 degree. To break the disulfide bonds of HER2 present on HEK293T cells, cells were cultured in the  
198 media containing 1 mM DTT for 1, 5, and 24 hours, and reactivities of the antibody were investigated  
199 by flow cytometry (Figure 4A). Remarkably, binding of H<sub>2</sub>Mab-214 was increased more than 2-fold  
200 after the 1-hour treatment with DTT, indicating that the number of epitope-bearing species increased  
201 due to the partial reduction of disulfide bonds. Furthermore, this increase was transient because the  
202 binding became less pronounced after 5 hours and returned to the basal level (without DTT treatment)  
203 after 24 hours. In sharp contrast, H<sub>2</sub>Mab-119 exhibited completely opposite behavior to the DTT-  
204 treatment; the binding was reduced by >95% after 1-hour DTT treatment, followed by the gradual  
205 recovery over time, returning to the basal level after 24 hours (Figure 4B). These observations are  
206 consistent with the idea that brief incubation with DTT induces partial disruption of the tertiary  
207 structure of HER2, which is favored by H<sub>2</sub>Mab-214 but disfavored by H<sub>2</sub>Mab-119, while the normal  
208 structure is restored as the effective concentration of DTT goes down by oxidation during the cell  
209 culture at 37°C.

210 To generalize the above notion, reactivities of four regular anti-HER2 mAbs, H<sub>2</sub>Mab-19 (epitope:  
211 domain III),<sup>40</sup> H<sub>2</sub>Mab-181 (epitope: domain III),<sup>41</sup> H<sub>2</sub>Mab-41 (epitope: domain IV),<sup>42</sup> and trastuzumab  
212 (epitope: domain IV), with HEK293T cells were investigated 1 and 24 hours after the addition of 1  
213 mM DTT. As in the case of H<sub>2</sub>Mab-119, all antibodies showed a markedly reduced reactivity with the  
214 cells at 1 hour, and that was nearly recovered at 24 hours (Figure S3). The decreased binding of non-  
215 cancer-specific mAbs with epitopes in different domains upon addition of DTT suggests that structural  
216 disruption occurred throughout the HER2 molecule. These results again highlight the unique character

217 of H<sub>2</sub>Mab-214 in that it recognizes structurally disrupted HER2.

218 If the reactivity of H<sub>2</sub>Mab-214 is governed by the partially unfolded nature of HER2 molecules  
219 on cell surface, the DTT-induced binding upregulation should be seen in any cell types. In fact, DTT  
220 treatment of normal mammary gland epithelial cell line MCF 10A resulted in small but statistically  
221 significant ( $p < 0.05$ ) increase in the reactivity of H<sub>2</sub>Mab-214 (Figure 4C). Furthermore, the same  
222 treatment also upregulated H<sub>2</sub>Mab-214 reactivity toward SK-BR-3 cells which were already positive  
223 for H<sub>2</sub>Mab-214 binding before the DTT treatment (Figure 4D), indicating that there is a pool of  
224 H<sub>2</sub>Mab-214-negative HER2 molecules expressed on breast cancer cells which can be converted to  
225 H<sub>2</sub>Mab-214-positive ones upon DTT treatment.

226

### 227 *Effects of targeted disruption of domain IV disulfide bond on the epitope exposure.*

228 Although the DTT treatment facilitated the conversion of HER2 domain IV to the alternative  
229 conformation reactive with H<sub>2</sub>Mab-214, it severely reduced the binding of all other mAbs, indicating  
230 that the DTT-treated HER2 has globally disturbed structure that does not accurately capture the  
231 character of H<sub>2</sub>Mab-214-reactive species on cancer cells. Considering the fact that most anti-HER2  
232 mAbs do not show cell-type specificity like H<sub>2</sub>Mab-214, cancer-specific HER2 structural alteration  
233 may be restricted to domain IV, particularly the region encompassing residues 612-618. We therefore  
234 set out to investigate whether targeted local disruption of this region via removing individual disulfide  
235 linkage can mimic cancer-specific presentation of the H<sub>2</sub>Mab-214 epitope. As the H<sub>2</sub>Mab-214 epitope  
236 is located between the 8th and 9th disulfide bonds in the domain IV (Figure 4E), we chose to remove  
237 the 6th to 10th disulfide bonds (C567:C584, C587:C596, C600:C623, C626:C634, and C630:C642),  
238 which are relatively close to the epitope. As a control, the first disulfide bond (C511:C520) which is  
239 ~55 Å away from the epitope was also removed. To remove individual disulfide bond, the pairing  
240 cysteine residues were simultaneously replaced with alanine in the context of full-length HER2. Upon  
241 the transient expression in CHO-K1 cells, their reactivities against the anti-HER2 antibodies were  
242 evaluated by flow cytometry.

243 As expected, H<sub>2</sub>Mab-119 reacted with all mutants at levels nearly equivalent to the wild-type,  
244 confirming the structural integrity at the domain I in these domain IV-mutants. Trastuzumab showed  
245 greatly reduced reactivity with the C567A/C584A and C587A/C596A mutants and moderately  
246 reduced reactivity with the C600A/C623A mutant, but binding to other mutants remained intact  
247 (Figure 4F). The epitope for trastuzumab is composed of three loops, Pro579-Gln583 (loop 1),  
248 Asp592-Phe595 (loop 2), and Lys615-Pro625 (loop 3) (Figure S1B). Structurally, the C567:C584 and  
249 C587:C596 disulfide bonds are located behind the loop 1 and 2, respectively, and appear to support  
250 the conformation of these loops, and the C600:C623 is located in a linker connecting the loop 2 and  
251 3. Thus, the reduced binding of trastuzumab in their removal correlates well with the structural  
252 observations. When the same set of HER2 mutants were evaluated for the binding by H<sub>2</sub>Mab-214,

253 however, they showed increased binding at varying degrees (from 30 to 90%), except for the pair  
254 located away from the epitope (i.e., C511:C520) (Figure 4F). This result indicates that the exposure  
255 of H<sub>2</sub>Mab-214 epitope does not require global misfolding of HER2 but can be facilitated by any local  
256 destabilization of the structure near the Pro612-Asp618 segment, which serves as a "weak ankle" of  
257 HER2 that readily changes its conformation into an alternative one.

258

#### 259 ***ADCC and CDC by H<sub>2</sub>Mab-214-mG<sub>2a</sub>-f against BT-474 and MDA-MB-468 cells.***

260 The high selectivity of H<sub>2</sub>Mab-214 for cancer cells could be a major advantage in its  
261 pharmaceutical application. Therefore, we evaluated the potential application of H<sub>2</sub>Mab-214 in cancer  
262 therapy. We have previously demonstrated that class-switched (from IgG<sub>1</sub> to IgG<sub>2a</sub>) and defucosylated  
263 mAbs exert potent antitumor effects in several mouse xenograft models.<sup>43-50</sup> To evaluate the antitumor  
264 activity of H<sub>2</sub>Mab-214 and H<sub>2</sub>Mab-119, class-switched and defucosylated mAbs (H<sub>2</sub>Mab-214-mG<sub>2a</sub>-  
265 f and H<sub>2</sub>Mab-119-mG<sub>2a</sub>-f) were produced by combining their V<sub>H</sub> with C<sub>H</sub> of mouse IgG<sub>2a</sub> (Figure S4A).  
266 We confirmed that H<sub>2</sub>Mab-214-mG<sub>2a</sub>-f and H<sub>2</sub>Mab-119-mG<sub>2a</sub>-f recognized BT-474, but not MDA-  
267 MB-468 cells (Figure S4B). As a defucosylated control mouse IgG<sub>2a</sub> mAb, we used 281-mG<sub>2a</sub>-f (anti-  
268 hamster podoplanin [PDPN] mAb), which never recognized BT-474 nor MDA-MB-468 cells (Figure  
269 S4B).

270 We first investigated whether H<sub>2</sub>Mab-214-mG<sub>2a</sub>-f and H<sub>2</sub>Mab-119-mG<sub>2a</sub>-f could exert ADCC  
271 against BT-474 cells. As shown in Figure 5A, H<sub>2</sub>Mab-214-mG<sub>2a</sub>-f showed ADCC activity (48.0%  
272 cytotoxicity) against BT-474 cells more potently than did the control mouse IgG<sub>2a</sub> (4.4% cytotoxicity;  
273 P<0.01) and 281-mG<sub>2a</sub>-f (4.8% cytotoxicity; P<0.01), and the activity was comparable to that induced  
274 by H<sub>2</sub>Mab-119-mG<sub>2a</sub>-f (43.6% cytotoxicity). We also investigated CDC activities of H<sub>2</sub>Mab-214-  
275 mG<sub>2a</sub>-f and H<sub>2</sub>Mab-119-mG<sub>2a</sub>-f against BT-474 cells. As shown in Figure 5B, both antibodies  
276 exhibited similar levels of CDC in BT-474 cells (H<sub>2</sub>Mab-214-mG<sub>2a</sub>-f: 76.5% cytotoxicity, H<sub>2</sub>Mab-  
277 119-mG<sub>2a</sub>-f: 72.1% cytotoxicity), which were significantly higher than that induced by control mouse  
278 IgG<sub>2a</sub> (9.5% cytotoxicity; P<0.01) and 281-mG<sub>2a</sub>-f (17.3% cytotoxicity; P<0.01). There were no  
279 differences between H<sub>2</sub>Mab-119-mG<sub>2a</sub>-f or H<sub>2</sub>Mab-214-mG<sub>2a</sub>-f and control mouse IgG<sub>2a</sub> or 281-mG<sub>2a</sub>-  
280 f in ADCC (Figure 5C) and CDC (Figure 5D) against MDA-MB-468 cells. These results demonstrated  
281 that H<sub>2</sub>Mab-214-mG<sub>2a</sub>-f exhibited ADCC and CDC comparable to H<sub>2</sub>Mab-119-mG<sub>2a</sub>-f against HER2-  
282 positive BT-474 cells, despite its reduced reactivity in flow cytometry (Figure 1).

283

#### 284 ***Antitumor effects of H<sub>2</sub>Mab-214-mG<sub>2a</sub>-f in BT-474 xenografts.***

285 We next investigated antitumor effects of the antibodies in BT-474 xenograft mouse models.  
286 H<sub>2</sub>Mab-119-mG<sub>2a</sub>-f, H<sub>2</sub>Mab-214-mG<sub>2a</sub>-f, control normal mouse IgG, or 281-mG<sub>2a</sub>-f were injected  
287 intraperitoneally on days 7, 14, and 19, after the inoculation of BT-474. The tumor volume was  
288 measured on days 7, 12, 14, 19, 22, and 26 after the inoculation. Administration of H<sub>2</sub>Mab-119-mG<sub>2a</sub>-f

289 and H<sub>2</sub>Mab-214-mG<sub>2a</sub>-f significantly reduced tumor volume compared to that of control normal mouse  
290 IgG in the BT-474 xenograft models after days 14 and 19, respectively (Figure 6A). The reduction in  
291 tumor volume on day 26 in mice treated with H<sub>2</sub>Mab-119-mG<sub>2a</sub>-f and H<sub>2</sub>Mab-214-mG<sub>2a</sub>-f was 41%  
292 and 35%, respectively, compared to mice treated with the control normal mouse IgG. In addition, as  
293 shown in Figure 6B, tumors from the H<sub>2</sub>Mab-119-mG<sub>2a</sub>-f and H<sub>2</sub>Mab-214-mG<sub>2a</sub>-f-treated mice  
294 weighed significantly less than those from control normal mouse IgG-treated mice (60% reduction;  
295 P<0.01 and 72% reduction, respectively; P<0.01). The reduction in tumor volume and weight in  
296 H<sub>2</sub>Mab-119-mG<sub>2a</sub>-f- and H<sub>2</sub>Mab-214-mG<sub>2a</sub>-f-treated mice was also significant compared to 281-  
297 mG<sub>2a</sub>-f-treated mice (Figures 6A and 6B). As a control experiment, the antitumor effects were also  
298 investigated in the MDA-MB-468 xenograft models. As a result, no difference was observed between  
299 H<sub>2</sub>Mab-119-mG<sub>2a</sub>-f or H<sub>2</sub>Mab-214-mG<sub>2a</sub>-f and control normal mouse IgG or 281-mG<sub>2a</sub>-f in both tumor  
300 volume (Figure S5A) and weight (Figure S5B), confirming that the antitumor effects observed in the  
301 BT-474 xenograft models were HER2-dependent.

302 Tumors that were resected from mice on day 26 are demonstrated in Figures 6C and S5C. The  
303 body weight loss was not observed in both H<sub>2</sub>Mab-119-mG<sub>2a</sub>-f and H<sub>2</sub>Mab-214-mG<sub>2a</sub>-f treated mice  
304 (Figures 6D and S5D). The mice on day 26 about BT-474 xenograft and MDA-MB-468 xenograft  
305 were demonstrated in Figures S6A and S6B, respectively.

306

## 307 **Discussion**

308 Trastuzumab is a pioneer in molecular targeted therapy and has been the most effective treatment  
309 for HER2-positive breast cancer for more than 20 years since its FDA approval in 1998.<sup>51</sup> The success  
310 of trastuzumab has demonstrated the utility of antibody drugs in cancer therapy, and mAbs have  
311 become one of the leading modalities in this field. As of 2018 (i.e., before COVID-19), half of the top  
312 10 best-selling antibody drugs were reported to be against cancer.<sup>52</sup> More recently, attention has  
313 focused on the development of more innovative mAb-based therapeutic strategies, such as antibody-  
314 drug conjugates (ADCs), chimeric antigen receptor (CAR)-T cell therapy, and bispecific antibodies.  
315 For HER2-positive metastatic breast cancer, the ADCs, trastuzumab emtansine and trastuzumab  
316 deruxtecan, have already been developed. With the trend shifting toward such therapies with high cell-  
317 killing activity, antibodies with high specificity for cancer cells are becoming increasingly important.  
318 In the development of therapeutic antibodies against cancers, efforts are being made to identify unique  
319 characteristics of cancer cells. A major strategy is to identify molecules that are highly expressed on  
320 the surface of certain types of cancer cells and have a high cancer cell/normal cell ratio as HER2.  
321 However, many of the molecules that are abnormally expressed on cancer cells have already been  
322 identified by extensive transcriptome and proteome analyses, making exploration for new cancer  
323 antigens very challenging. In addition, in this strategy, the target molecules are common autoantigens  
324 that are also expressed on normal cells, raising concerns about adverse effects caused by antibody

325 drugs.

326 In this study, we succeeded in developing the highly cancer-specific mAb targeting HER2. The  
327 reactivity of H<sub>2</sub>Mab-214 against cancer cells was clearly observed, whereas that against normal cells  
328 was not detectable even by flow cytometry, which is a highly sensitive detection system (Figure 1).  
329 The cancer specificity of H<sub>2</sub>Mab-214 was found to be due to the recognition of a structural feature that  
330 only HER2 on cancer cells has, namely the misfolded region. Previously, cancer-specific antibodies  
331 that appear to recognize structural features of target molecules, anti-EGFR antibody mAb806 and anti-  
332  $\alpha\beta 7$  integrin antibody MMG49, have been reported.<sup>53,54</sup> Their cancer specificity is, however, thought  
333 to be linked to the global conformation of their target molecules rather than to local structural features.  
334 More specifically, their epitopes are expected to be hidden on normal cells but exposed on cancer cells  
335 for some reason. For mAb806, it has also been demonstrated by crystallographic analysis that the  
336 antigen peptide bound to the antibody has almost the same conformation as the corresponding region  
337 in the EGFR.<sup>55</sup> By contrast, H<sub>2</sub>Mab-214 is a new type of cancer-specific mAb that directly recognizes  
338 the unique structural feature of the target. In the current crystal structure, the epitope peptide (Met611-  
339 Asp618) assumes U-shaped conformation nestled in the binding pocket of H<sub>2</sub>Mab-214, which is not  
340 compatible with the canonical conformation seen in the native HER2 reported so far. As the segment  
341 is part of a rigid 3-strand  $\beta$ -sheet in the native structure, the HER2 species reactive with H<sub>2</sub>Mab-214  
342 must have undergone local misfolding at this region to allow the access of the antibody. Therefore,  
343 H<sub>2</sub>Mab-214-reactive HER2 on cancer cells and H<sub>2</sub>Mab-214-non-reactive HER2 on normal cells are  
344 chemically identical molecules having a subtle conformational difference present in a restricted region  
345 near the Pro612-Asp618 (Figures 5G and 5H).

346 Proteins are inherently prone to misfold. Homeostasis of membrane and secretory proteins is  
347 normally maintained by quality control system in the endoplasmic reticulum (ER), but cancer cells are  
348 constantly exposed to a variety of stressors such as oxidative stress, hypoxia, and decreased energy  
349 supply, which are known to promote production and accumulation of misfolded proteins in the ER  
350 (called ER stress).<sup>56</sup> We speculate that in such an abnormal condition of the ER in cancer cells, proteins  
351 with minor structural defects (such as a misformation of a disulfide bond that does not impair overall  
352 domain stability or function) may escape the quality control system and are transported normally,  
353 presenting a cancer-specific "mark" to the immune system. Since our study showed that the  
354 conformational integrity of HER2 at residues 612 to 618 is susceptible to the lack of surrounding  
355 disulfide bonds, the local misfolding of HER2 may have stemmed from the dysregulated redox system  
356 in the ER of cancer cells. In breast cancer cells, it has been reported that the expression of protein  
357 disulfide isomerases (PDI), PDIA1, PDIA3, PDIA4, and PDIA6, is elevated, suggesting an abnormal  
358 state of the redox system in the ER.<sup>57</sup> Disruption of disulfide bond formation in cancer cells has also  
359 been proposed for EGFR.<sup>55</sup>

360 As far as we are aware, only H<sub>2</sub>Mab-214 shows cancer specificity among the many anti-HER2

361 antibodies developed to date, including trastuzumab that recognizes a region very close to the H<sub>2</sub>Mab-  
362 214 epitope. Therefore, the H<sub>2</sub>Mab-214 epitope (Pro612-Asp618 region) may be very special in that  
363 it undergoes spatially confined misfolding to expose highly antigenic peptide in cancer cells.  
364 Surprisingly, when we immunized mice with a synthetic peptide containing the H<sub>2</sub>Mab-214 epitope  
365 sequence, all mAbs obtained were found to show cancer specificity (data not shown). This suggests  
366 that prior knowledge about the misfold-dependent cancer neoantigen sequence may be leveraged to  
367 obtain useful cancer-specific mAbs. By using such strategy, it may be possible to establish H<sub>2</sub>Mab-  
368 214-like antibodies that are more suitable for therapeutic applications, such as fully human mAbs or  
369 high-affinity mAbs. As evidenced by the performance of trastuzumab, the lower stalk region of HER2  
370 should also be a promising target in terms of the therapeutic efficacy. In fact, even though not all  
371 HER2 molecules on cancer cells are H<sub>2</sub>Mab-214 reactive, H<sub>2</sub>Mab-214 showed anti-tumor activity  
372 comparable to the pan-HER2 reactive H<sub>2</sub>Mab-119 (Figures 4 and 6). More importantly, the high  
373 cancer specificity is of great benefit in applications where very high therapeutic efficacy is expected,  
374 such as CAR-T cell therapy and bispecific antibodies.

375 HER2 has a long history as a successful cancer therapeutic target and has been well studied, yet  
376 its unique and cancer-specific structural defect that can be targeted by mAb had not been discovered  
377 until now. Our results indicate that some molecules that had not been considered as good cancer-  
378 specific therapeutic target due to the widespread expression in many tissues may in fact become viable  
379 drug target if they are found to undergo cancer-specific local misfolding. It is hoped that the expansion  
380 of potential targets will facilitate the development of mAb therapies for cancers for which effective  
381 treatments have not yet been found.

382

### 383 **Acknowledgements**

384 We would like to thank the staff of the beamline at SPring-8 for their help with X-ray data  
385 collection. This work was supported in part by JSPS KAKENHI grant numbers JP21H02416 to T.A.  
386 and JP22K07224 to Y.K. from Japan Society for the Promotion of Science, by the Research Support  
387 Project for Life Science and Drug Discovery (Basis for Supporting Innovative Drug Discovery and  
388 Life Science Research (BINDS)) from Japan Agency for Medical Research and Development  
389 (AMED) under grant numbers JP22ama121011 to J.T. and JP22ama121008 to Y.K., and also  
390 supported by AMED under grant numbers JP22am0401013 to Y.K., 23bm1123027h0001 to Y.K., and  
391 JP22ck0106730 to Y.K.

392

### 393 **Author contributions**

394 T.A. designed and performed experiments, analyzed the data, and wrote the manuscript. E.M.,  
395 H.S., T.O., T.T., and M.K.K. performed experiments and analyzed the data. J.T. and Y.K. conceived  
396 the experimental design, analyzed the data, and wrote the manuscript. All authors contributed to the

397 preparation of the manuscript.

398

### 399 **Declaration of interests**

400 Mika K. Kaneko and Yukinari Kato submitted a patent application related to this work: H<sub>2</sub>Mab-  
401 214. Patent application number WO2022114163. (2021). The remaining authors declare no competing  
402 interests.

403

### 404 **Figure legends**

405

406 **Figure 1. Flow cytometry using trastuzumab, H<sub>2</sub>Mab-119, and H<sub>2</sub>Mab-214.** (A) CHO-K1 and  
407 CHO/HER2 cells were treated with 10 µg/ml of trastuzumab, H<sub>2</sub>Mab-119, and H<sub>2</sub>Mab-214 or buffer  
408 control. (B) BT-474, MDA-MB-468, SK-BR-3, HEK293T, HaCaT, and MCF 10A cells were treated  
409 with 10 µg/ml of trastuzumab, H<sub>2</sub>Mab-119, H<sub>2</sub>Mab-214 or buffer control. Then, cells were stained  
410 with Alexa Fluor 488-conjugated anti-mouse IgG (for H<sub>2</sub>Mab-119 and H<sub>2</sub>Mab-214) or FITC-  
411 conjugated anti-human IgG (for trastuzumab). The black line represents the negative control (blocking  
412 buffer).

413

414 **Figure 2. Epitope mapping of H<sub>2</sub>Mab-214.** (A) Domain organization of HER2 and design of a series  
415 of N-terminal domain deletion mutants used for the flow cytometry analysis. (B) Binding of H<sub>2</sub>Mab-  
416 214 and H<sub>2</sub>Mab-119 to the deletion mutants of HER2 transiently expressed on CHO-K1 cells. CHO-  
417 K1 cells expressing each mutant were treated with NZ-1, H<sub>2</sub>Mab-214, H<sub>2</sub>Mab-119, or buffer control  
418 (black line), stained with Alexa Fluor 488-conjugated secondary antibodies, and analyzed in flow  
419 cytometry. (C-E) Evaluation of reactivity of H<sub>2</sub>Mab-214 toward various HER2-derived synthetic  
420 peptides by ELISA. 10 µg/ml of H<sub>2</sub>Mab-214 was incubated with wells coated with the synthetic  
421 peptides, followed by incubation with peroxidase-conjugated anti-mouse antibodies. The optical  
422 density was measured at 655 nm. Data are from one experiment (C) or from one triplicate experiment  
423 (D and E; mean ± SEM). N.C., negative control.

424

425 **Figure 3. Structural analysis of H<sub>2</sub>Mab-214.** (A) Close-up view of the antigen binding site in the  
426 crystal structure of H<sub>2</sub>Mab-214 complexed with the epitope peptide. H<sub>2</sub>Mab-214 is shown as a surface  
427 model, and the epitope peptide is shown as a stick model with a transparent sphere model. (B)  
428 Hydrogen bonding interactions observed between H<sub>2</sub>Mab-214 and the epitope peptide. Hydrogen  
429 bonds are denoted by dashed lines. Water molecules are shown as sphere models. (C) Crystal structure  
430 of H<sub>2</sub>Mab-119 complexed with the HER2 domain I fragment. The domain I is shown as a cyan cartoon  
431 model, and the H<sub>2</sub>Mab-119 is shown as a cartoon model with a transparent surface model. HER2  
432 residues in contact with the H<sub>2</sub>Mab-119 (within 4 Å) are indicated in magenta. (D) Overall structure

433 of the HER2 ectodomain (PDB ID: 3n85). Met611-Asp618 region is colored in yellow. An expanded  
434 view of the region indicated by the black box is shown on the right. The C $\alpha$  atoms of the residues 611-  
435 618 are shown as spheres and disulfide bonds are shown as red stick models. (E-H) Structural  
436 comparison of the Met611-Asp618 region in the HER2 ectodomain (E; crystal structure and G;  
437 schematic diagram) and the peptide bound to H<sub>2</sub>Mab-214 (F; crystal structure and H; schematic  
438 diagram).

439

440 **Figure 4. Analysis of antibody binding upon disulfide bond breakage in HER2.** (A,B) Flow  
441 cytometry analysis of DTT-treated HEK293T cells. HEK293T cells were pre-treated with 1 mM DTT  
442 for 1, 5, or 24 hours and then stained with H<sub>2</sub>Mab-214 (A), H<sub>2</sub>Mab-119 (B), or buffer control, followed  
443 by flow cytometry analysis. Line graphs of the median fluorescence intensity (MFI) values are provided  
444 on the right side of the histograms. (C, D) Effect of DTT treatment of MCF 10A (C) and SK-BR-3  
445 (D) cells on antibody binding. MCF 10A and SK-BR-3 cells were either untreated or pre-treated with  
446 1 mM DTT for 1 hour and then stained with H<sub>2</sub>Mab-214, H<sub>2</sub>Mab-119, or buffer control, followed by  
447 flow cytometry analysis. Results are reported as fold change in MFI compared with the buffer control.  
448 Data are mean + SEM of four independent experiments. *P* values were calculated using unpaired one-  
449 tailed t-test. \**P*<0.05, \*\**P*<0.01. \*\*\**P*<0.001. (E) HER2 domain IV structure extracted from 3n85.  
450 The disulfide bonds are indicated by red sticks. (F) Binding of antibodies to the disulfide bond removal  
451 HER2 mutants. CHO-K1 cells transiently expressing each mutant were stained with H<sub>2</sub>Mab-119,  
452 trastuzumab, or H<sub>2</sub>Mab-214 and analyzed in flow cytometry. Relative impact of each mutation on  
453 binding is expressed as the fold change in the % positive cells from the wild-type after normalizing  
454 the expression level of each mutant using the NZ-1-stained cells. Signals from cells transfected with  
455 empty vectors were used to define antibody-bound cell populations (regions including <1% of cells  
456 transfected with empty vectors were used for the calculation of % positive cells). Data are mean ±  
457 SEM of three independent experiments.

458

459 **Figure 5. H<sub>2</sub>Mab-119-mG<sub>2a</sub>-f- and H<sub>2</sub>Mab-214-mG<sub>2a</sub>-f-mediated ADCC and CDC against BT-  
460 474 (HER2-positive) and MDA-MB-468 (TNBC) cells.** (A, C) ADCC induced by H<sub>2</sub>Mab-119-  
461 mG<sub>2a</sub>-f, H<sub>2</sub>Mab-214-mG<sub>2a</sub>-f, control mouse IgG<sub>2a</sub> or 281-mG<sub>2a</sub>-f against BT-474 (A) and MDA-MB-  
462 468 (C) cells. (B,D) CDC induced by H<sub>2</sub>Mab-119-mG<sub>2a</sub>-f, H<sub>2</sub>Mab-214-mG<sub>2a</sub>-f, control mouse IgG<sub>2a</sub>  
463 or 281-mG<sub>2a</sub>-f against BT-474 (B) and MDA-MB-468 (D) cells. Values are shown as mean ± SEM.  
464 Asterisks indicate statistical significance (\*\**p*<0.01; Welch's *t*-test). ADCC, antibody-dependent  
465 cellular cytotoxicity; CDC, complement-dependent cytotoxicity.

466

467 **Figure 6. Antitumor activity of H<sub>2</sub>Mab-119-mG<sub>2a</sub>-f and H<sub>2</sub>Mab-214-mG<sub>2a</sub>-f against BT-474  
468 xenograft.** (A) BT-474 cells (5 × 10<sup>6</sup> cells) were subcutaneously injected into BALB/c nude mice. On

469 day 7, 100  $\mu$ g of H<sub>2</sub>Mab-119-mG<sub>2a</sub>-f, H<sub>2</sub>Mab-214-mG<sub>2a</sub>-f, control normal mouse IgG or 281-mG<sub>2a</sub>-f  
 470 were injected intraperitoneally into mice. Additional antibodies were injected on days 14 and 19. The  
 471 tumor volume was measured on days 7, 12, 14, 19, 22, and 26 after the inoculation of BT-474. Values  
 472 are presented as the mean  $\pm$  SEM. \*P<0.05, \*\*P<0.01 (ANOVA and Tukey's multiple comparisons  
 473 test). (B) Tumor weight (day 26) was measured from excised BT-474 xenograft tumors. Values are  
 474 presented as the mean  $\pm$  SEM. \*\*P<0.01 (Welch's *t* test). (C) Appearance of BT-474 xenograft tumors  
 475 from the H<sub>2</sub>Mab-119-mG<sub>2a</sub>-f, H<sub>2</sub>Mab-214-mG<sub>2a</sub>-f, control normal mouse IgG and 281-mG<sub>2a</sub>-f-treated  
 476 mice on day 26 (scale bar, 1 cm). (D) Mice weight in H<sub>2</sub>Mab-119-mG<sub>2a</sub>-f, H<sub>2</sub>Mab-214-mG<sub>2a</sub>-f, control  
 477 normal mouse IgG and 281-mG<sub>2a</sub>-f-treated groups. n.s., not significant.

478

479

480 **Table 1 The main chain dihedral angles.**

residue	Phi/Psi angles (°) in the HER2 ectodomain structures		Phi/Psi angles (°) in the H <sub>2</sub> Mab-214 Fv-clasp/epitope peptide complex
	(PDB: 3n85)	(PDB: 6j71)	
Pro612	-60.9/143.0	-86.6/138.7	-62.7/149.5
Ile613	-104.1/113.8	-91.2/117.5	-106.6/102.1
Trp614	-107.3/128.4	-114.7/112.1	-76.7/-38.3
Lys615	-138.3/166.5	-133.8/170.7	-109.5/-112.4
Phe616	-141.6/152.4	-147.6/157.1	-110.6/161.9
Pro617	-78.1/160.6	-66.4/159.1	-53.0/125.4

481

482

### 483 **STAR Methods**

#### 484 **Resource availability**

485

#### 486 **Lead contact**

487 Further information and requests for resources and reagents should be directed to and will be  
 488 fulfilled by the lead contact, Takao Arimori (arimori@protein.osaka-u.ac.jp).

489

#### 490 **Materials availability**

491 H<sub>2</sub>Mab-214 is available from Tohoku University Graduate School of Medicine.

492

#### 493 **Method details**

##### 494 *Cell lines*

495 Chinese hamster ovary (CHO)-K1, BT-474, SK-BR-3, MDA-MB-468, HEK293T, and MCF  
 496 10A cell lines were obtained from the American Type Culture Collection (ATCC). HaCaT cell line

497 was obtained from Cell Lines Service GmbH (Eppelheim). CHO/HER2 were generated by transfecting  
498 pCAG/PA-HER2-RAP-MAP into CHO-K1 cells using Lipofectamine LTX (Thermo Fisher Scientific,  
499 Inc.). A few days after transfection, PA tag-positive cells were sorted by a cell sorter (SH800; Sony  
500 Corp.) using NZ-1, which was originally developed as an anti-human PDPN mAb.<sup>58</sup>

501 CHO-K1 and CHO/HER2 were cultured in RPMI-1640 medium (Nacalai Tesque, Inc.) or in  
502 Ham's F-12 medium (FUJIFILM Wako Pure Chemical Corporation), and BT-474, SK-BR-3, MDA-  
503 MB-468, HEK293T, and HaCaT were cultured in DMEM medium (Nacalai Tesque, Inc.),  
504 supplemented with 10% heat-inactivated fetal bovine serum (FBS; Thermo Fisher Scientific Inc.), 100  
505 units/ml of penicillin, 100 µg/ml streptomycin, and 0.25 µg/ml amphotericin B (Nacalai Tesque, Inc.).  
506 MCF 10A was cultured in Mammary Epithelial Cell Basal Medium BulletKit™ (CC-3150, Lonza)  
507 supplemented with 100 ng/ml cholera toxin (Sigma-Aldrich). All cell lines were cultured at 37°C in a  
508 humidified atmosphere with 5% CO<sub>2</sub> and 95% air.

509

#### 510 *Antibodies*

511 Anti-HER2 mAb, H<sub>2</sub>Mab-119 (IgG<sub>1</sub>, kappa), was established as previously described.<sup>36</sup> H<sub>2</sub>Mab-  
512 214 (IgG<sub>1</sub>, kappa) was established by the same strategy. In brief, BALB/c mice were immunized with  
513 recombinant HER2-extracellular domain produced by LN229 cells together with Imject Alum  
514 (Thermo Fisher Scientific, Inc.). After several additional immunizations, spleen cells were fused with  
515 P3U1 cells. The culture supernatants of hybridomas were screened using enzyme-linked  
516 immunosorbent assay with recombinant HER2-extracellular domain and flow cytometry.

517 Variable (V<sub>H</sub>) and constant (C<sub>H</sub>) regions of heavy chain cDNAs of H<sub>2</sub>Mab-119 and H<sub>2</sub>Mab-214  
518 were subcloned into the pCAG-Neo vector (FUJIFILM Wako Pure Chemical Corporation). Variable  
519 (V<sub>L</sub>) and constant (C<sub>L</sub>) regions of light chain cDNAs of H<sub>2</sub>Mab-119 and H<sub>2</sub>Mab-214 were subcloned  
520 into the pCAG-Ble vector (FUJIFILM Wako Pure Chemical Corporation). To produce recombinant  
521 H<sub>2</sub>Mab-119 and H<sub>2</sub>Mab-214, the vectors of heavy and light chains were transfected into ExpiCHO-S  
522 cells using the ExpiCHO Expression System (Thermo Fisher Scientific Inc.). H<sub>2</sub>Mab-119 and H<sub>2</sub>Mab-  
523 214 were purified using Ab-Capcher (ProteNova Co., Ltd.).

524 To generate H<sub>2</sub>Mab-119-mG<sub>2a</sub>-f and H<sub>2</sub>Mab-214-mG<sub>2a</sub>-f, we subcloned these V<sub>H</sub> cDNA and C<sub>H</sub>  
525 of mouse IgG<sub>2a</sub> into the pCAG-Ble vector. These V<sub>L</sub> cDNA and C<sub>L</sub> cDNA of mouse kappa light chain  
526 were also subcloned into the pCAG-Neo vector. The vectors for the H<sub>2</sub>Mab-119-mG<sub>2a</sub> or H<sub>2</sub>Mab-214-  
527 mG<sub>2a</sub> were transduced into BINDS-09 (FUT8-knockout ExpiCHO-S) cells, and recombinant mAbs  
528 were produced using the ExpiCHO Expression System. H<sub>2</sub>Mab-119-mG<sub>2a</sub>-f and H<sub>2</sub>Mab-214-mG<sub>2a</sub>-f  
529 were purified using Ab-Capcher. Preparation of 281-mG<sub>2a</sub>-f (defucosylated anti-hamster PDPN mAb,  
530 control defucosylated mouse IgG<sub>2a</sub>) was previously described.<sup>43</sup> Trastuzumab (Herceptin) was  
531 obtained from Chugai Pharmaceutical Co., Ltd (Tokyo, Japan).

532

533 *Animal Experiments*

534 The animal experiment for generation of anti-HER2 mAbs was approved by the Animal Care and  
535 Use Committee of Tohoku University (Permit number: 2019NiA-001). Animal experiments for  
536 ADCC and antitumor activity were approved by the Institutional Committee for Experiments of the  
537 Institute of Microbial Chemistry (approval no. 2023-001 and 2023-018). Mice were maintained and  
538 monitored as described previously.<sup>59</sup> The loss of original body weight was determined to a point >25%  
539 and/or a maximum tumor size >3,000 mm<sup>3</sup> as humane endpoints for euthanasia.

540

541 *Flow cytometry*

542 CHO-K1, CHO/HER2, BT-474, SK-BR-3, MDA-MB-468, HEK293T, HaCaT, and MCF 10A  
543 cells were obtained using 0.25% trypsin and 1 mM ethylenediamine tetraacetic acid (EDTA; Nacalai  
544 Tesque, Inc.). The cells were treated with primary mAbs (H<sub>2</sub>Mab-119, H<sub>2</sub>Mab-214, H<sub>2</sub>Mab-119-mG<sub>2a</sub>-  
545 f, H<sub>2</sub>Mab-214-mG<sub>2a</sub>-f, or trastuzumab) or blocking buffer (control; 0.1% BSA in PBS) for 30 min at  
546 4°C. Then, the cells were treated with Alexa Fluor 488-conjugated anti-mouse IgG (1:1,000; Cell  
547 Signaling Technology, Inc.) or FITC-conjugated anti-human IgG (1:1,000; Sigma-Aldrich for  
548 trastuzumab) for 30 min at 4°C.

549 To analyze the antibody binding to DTT-treated cells, HEK293T, SK-BR-3, and MCF 10A cells  
550 were cultured in the media containing 1 mM DTT for an arbitrary time. The cells were then washed  
551 repeatedly with PBS to remove DTT and treated with 0.5 µg/ml of trastuzumab or 10 µg/ml of H<sub>2</sub>Mab-  
552 119, H<sub>2</sub>Mab-214, H<sub>2</sub>Mab-19, H<sub>2</sub>Mab-181, or H<sub>2</sub>Mab-41 for 1 hour on ice, followed by treatment with  
553 5 µg/ml of Alexa Fluor 488-conjugated anti-human IgG or anti-mouse IgG for 45 min on ice.

554 For the assessment of antibody binding to HER2 mutants, CHO-K1 cells were transiently  
555 transfected with vectors encoding various HER2 mutants or empty vector using X-tremeGENE HP  
556 DNA Transfection Reagent (Merck KGaA). The cells were stained with antibodies using the same  
557 procedure as for the DTT-treated cells.

558 All fluorescence data were collected using SA3800 Cell Analyzer (Sony Corp.) and analyzed  
559 using FlowJo (BD Biosciences).

560

561 *Enzyme-Linked Immunosorbent Assay (ELISA)*

562 NUNC Maxisorp 96-well plates (Thermo Fisher Scientific, Inc.) were coated with synthetic  
563 peptides (10 µg/ml; PepScreen by Sigma-Aldrich) or HER2ec (10 µg/ml) for 30 min at 37°C and  
564 blocked with Superblock reagent (Thermo Fisher Scientific, Inc.) or 1% bovine serum albumin  
565 (Nacalai Tesque, Inc.) in 0.05% Tween 20 containing PBS (1% BSA/PBST) for 30 min at 37°C.  
566 H<sub>2</sub>Mab-214 (10 µg/ml) was then added to the plate and incubated for 30 min at 37°C. To detect bound  
567 antibodies, horseradish peroxidase-conjugated rabbit anti-mouse IgG antibody (Agilent Technologies)  
568 diluted to 1:2,000 in 1% BSA/PBST was added and incubated for 30 min at 37°C. We used ELISA

569 POD Substrate TMB Kit (Nacalai Tesque, Inc.) for the enzymatic reactions. The optical density was  
570 measured at 655 nm using an iMark microplate reader (Bio-Rad Laboratories, Inc.).

571

572 *ADCC*

573 Splens were aseptically removed from six female BALB/c nude mice (five-week-old, Charles  
574 River Laboratories, Inc.) Single-cell suspensions were obtained using a cell strainer (352360, BD  
575 Biosciences). Erythrocytes were removed with the treatment of ice-cold distilled water. The  
576 splenocytes were used as effector cells.

577 H<sub>2</sub>Mab-119-mG<sub>2a</sub>-f and H<sub>2</sub>Mab-214-mG<sub>2a</sub>-f-mediated ADCC was assayed as follows. Target  
578 cells (BT-474 and MDA-MB-468) were labeled with 10 µg/ml Calcein AM (Thermo Fisher Scientific,  
579 Inc.). The target cells ( $2 \times 10^4$  cells) were plated in 96-well plates and mixed with effector cells  
580 (effector/target cells ratio, 50), 100 µg/ml of H<sub>2</sub>Mab-119-mG<sub>2a</sub>-f, H<sub>2</sub>Mab-214-mG<sub>2a</sub>-f, 281-mG<sub>2a</sub>-f  
581 (control defucosylated mouse IgG<sub>2a</sub>) or control mouse IgG<sub>2a</sub> (Sigma-Aldrich). Following incubation  
582 for 4.5 h at 37°C, the Calcein release into the medium was analyzed using a microplate reader (Power  
583 Scan HT; BioTek Instruments, Inc.) with an excitation wavelength (485 nm) and an emission  
584 wavelength (538 nm).

585 Cytotoxicity (% lysis) was calculated as follows: % lysis = (E - S)/(M - S) x 100, where “E” is  
586 the fluorescence in cultures of both effector and target cells, “S” is the spontaneous fluorescence of  
587 only target cells, and “M” is the maximum fluorescence following the treatment with a lysis buffer  
588 (10 mM Tris-HCl [pH 7.4], 10 mM EDTA, and 0.5% Triton X-100).

589

590 *CDC*

591 The Calcein AM- labeled target cells (BT-474 and MDA-MB-468) were plated in 96-well plates  
592 and mixed with rabbit complement (final dilution 1:10, Low-Tox-M Rabbit Complement; Cedarlane  
593 Laboratories) and 100 µg/ml of H<sub>2</sub>Mab-119-mG<sub>2a</sub>-f, H<sub>2</sub>Mab-214-mG<sub>2a</sub>-f, 281-mG<sub>2a</sub>-f or control  
594 mouse IgG<sub>2a</sub>. Following incubation for 4.5 h at 37°C, Calcein release into the medium was measured  
595 as indicated above.

596

597 *Antitumor activity of H<sub>2</sub>Mab-119-mG<sub>2a</sub>-f and H<sub>2</sub>Mab-214-mG<sub>2a</sub>-f in xenografts of BT-474 and MDA-*  
598 *MB-468 cells.*

599 BT-474 and MDA-MB-468 ( $5 \times 10^6$  cells) resuspended in DMEM and mixed with BD Matrigel  
600 Matrix Growth Factor Reduced (BD Biosciences) were subcutaneously injected into the left flank of  
601 BALB/c nude mice (Charles River Laboratories, Inc). On day 7 post-inoculation, 100 µg of H<sub>2</sub>Mab-  
602 119-mG<sub>2a</sub>-f (n=8), H<sub>2</sub>Mab-214-mG<sub>2a</sub>-f (n=8), 281-mG<sub>2a</sub>-f (n=8) or control mouse IgG (FUJIFILM  
603 Wako Pure Chemical Corporation) (n=8) in 100 µl PBS were intraperitoneally injected. On days 14  
604 and 19, additional antibody injections were performed. The tumor volume was measured on days 7,

605 12, 14, 19, 22, and 26 after the inoculation of cells. Tumor volumes were determined as previously  
606 described.<sup>59</sup>

607

### 608 *Statistical analyses*

609 All data are expressed as mean  $\pm$  standard error of the mean (SEM). Welch's t test was used for  
610 the statistical analyses in ADCC, CDC, and tumor weight. ANOVA with Tukey's post hoc test were  
611 used for the statistical analyses in tumor volume and mouse weight. GraphPad Prism 8 (GraphPad  
612 Software, Inc.) was utilized for the calculations.  $P < 0.05$  was considered to indicate a statistically  
613 significant difference.

614

### 615 *Crystallization*

616 To generate H<sub>2</sub>Mab-214 Fv-clasp, V<sub>H</sub> (residues 1-113) and V<sub>L</sub> (residues 1-108) regions of  
617 H<sub>2</sub>Mab-214 were appended to SARAH domain derived from human Mst1.<sup>39</sup> Hinge-less Fc (residues  
618 234-447 of human IgG1) was subsequently appended to the V<sub>L</sub>-SARAH. The DNA fragments were  
619 subcloned into the pcDNA3.1 vector (Thermo Fisher Scientific, Inc.). V<sub>H</sub>-SARAH and V<sub>L</sub>-SARAH-  
620 Fc were co-expressed in Expi293F cells (Thermo Fisher Scientific, Inc.) and purified with rProtein A  
621 Sepharose Fast Flow (Cytiva). The Fc portion was digested by treatment with a His-tagged IdeS  
622 protease for 2 hours at 37°C, followed by removal of His-IdeS by Ni-NTA Agarose (QIAGEN). The  
623 sample was further purified by anion-exchange chromatography on a MonoQ 5/50 GL column  
624 (Cytiva) equilibrated with 20 mM Tris, pH 8.0, and the resultant sample was concentrated by  
625 ultrafiltration using Amicon Ultra (Merck Millipore) and mixed with synthetic epitope peptide  
626 (residues 611-618 of HER2, MPIWKFPD) to be the final concentration of 5 mg/ml H<sub>2</sub>Mab-214 Fv-  
627 clasp and 0.6 mM peptide. To prepare the recombinant H<sub>2</sub>Mab-119 Fab, the V<sub>H</sub> to C<sub>H</sub>1 region of the  
628 H<sub>2</sub>Mab-119 heavy chain was subcloned into the pCAG-Neo vector and co-expressed with the H<sub>2</sub>Mab-  
629 119 light chain in ExpiCHO-S cells. H<sub>2</sub>Mab-119 Fab was purified with Capto L (Cytiva) followed by  
630 Protein G Sepharose 4 Fast Flow (Cytiva).

631 The HER2 domain I (residues 1-216) with a C-terminal His-tag was subcloned into pcDNA3.4  
632 (Thermo Fisher Scientific, Inc.) and expressed in Expi293F GnT1- cells (Thermo Fisher Scientific,  
633 Inc.), followed by purification with Ni-NTA Agarose. For the crystallization, H<sub>2</sub>Mab-119 Fab was  
634 mixed with HER2 domain I at 1.5-fold molar excess and subjected to size-exclusion chromatography  
635 (SEC) on a Superdex 200 Increase 10/300 GL column equilibrated with 20 mM Tris, 150 mM NaCl,  
636 pH 8.0 (Figure S2C). The purified sample was concentrated to 5 mg/ml by ultrafiltration using Amicon  
637 ultra (Merck Millipore).

638 Crystallization screening was carried out using The Classic Suite (QIAGEN), Wizard Classic 1 &  
639 2 (Rigaku), JCSG-plus (Molecular Dimensions), and ProPlex (Molecular Dimensions) crystallization  
640 reagents by using the sitting-drop vapor diffusion method at 20°C.

641

642 *Data collection, structure determination, and refinement*

643 Crystals of the H<sub>2</sub>Mab-214 Fv-clasp/epitope peptide complex obtained under the condition of 0.1  
644 M CHES pH 9.5, 20 % w/v polyethylene glycol (PEG) 8000 (JCSG plus, tube 1-7) and the H<sub>2</sub>Mab-  
645 119 Fab/HER2 domain I complex obtained under the condition of 0.1M Sodium citrate pH5.5, 20%  
646 w/v PEG3000 (JCSG plus, tube 1-2) were cryo-protected by well solution containing 15% PEG200  
647 and 30% PEG3000, respectively.

648 Diffraction data were collected at 100 K at beamline BL44XU of SPring-8 (Harima, Japan). The  
649 data were processed and scaled using X-ray Detector Software.<sup>60</sup> Initial phases were determined by  
650 molecular replacement with PHAER<sup>61</sup> in the CCP4 package<sup>62</sup> using the crystal structures deposited in  
651 Protein Data Bank (PDB) with IDs of 7cea (for H<sub>2</sub>Mab-214 V<sub>H</sub>), 7bsc (for H<sub>2</sub>Mab-214 V<sub>L</sub>), 7cea (for  
652 SARAH domain), 1f3d (for H<sub>2</sub>Mab-119 V<sub>H</sub>-C<sub>H1</sub>), 3wkm (for H<sub>2</sub>Mab-119 V<sub>L</sub>-C<sub>L</sub>), and 4hr1 (for HER2  
653 domain I) as search models. The structural models were modified with COOT,<sup>63</sup> refined with  
654 PHENIX,<sup>64</sup> and validated with MolProbity.<sup>65</sup> Data collection statistics and refinement parameters are  
655 summarized in Table S1.

656

657 **Data and code availability**

658 Coordinates for the structural models of H<sub>2</sub>Mab-214 Fv-clasp/epitope peptide complex and  
659 H<sub>2</sub>Mab-119 Fab/HER2 domain I complex have been deposited to the Protein Data Bank under PDB  
660 accession numbers 8jyq and 8jyr, respectively. All deposited data is publicly available as of the date  
661 of publication.

662 Any additional information required to reanalyze the data reported in this paper is available from  
663 the lead contact upon request.

664

665 **Supplemental information**

666

667 **Figure S1. Epitopes for H<sub>2</sub>Mab-214 and trastuzumab.** (A) Amino-acid sequence of the HER2  
668 domain IV. H<sub>2</sub>Mab-214 epitope region is shown in red. Cysteines with the disulfide linkages are  
669 connected by black lines. Residues forming a  $3_{10}$  helix and  $\beta$  strands are highlighted in pink and blue,  
670 respectively. *N*-glycosylation motifs are underlined, and residues in contact with trastuzumab (in  
671 7mn8) are indicated by asterisks. (B) Structure of the trastuzumab-bound HER2 ectodomain (extracted  
672 from 7mn8). An expanded view of the trastuzumab binding site is provided in the inset. HER2 residues  
673 in contact with the trastuzumab (within 4 Å) are shown as brown stick models. The H<sub>2</sub>Mab-214 epitope  
674 and disulfide bonds are colored in yellow and red, respectively.

675

676 **Figure S2. Structure determination of H<sub>2</sub>Mab-214 and H<sub>2</sub>Mab-119.** (A) Overall structure of  
677 H<sub>2</sub>Mab-214 Fv-clasp in complex with the epitope peptide. (B) Simulated-annealing  $F_o-F_c$  omit map  
678 for the H<sub>2</sub>Mab-214 antigen peptide (blue mesh, contoured at 3.0  $\sigma$  level). The assigned peptide model  
679 is shown as orange sticks. (C) Size-exclusion chromatography (SEC) analysis. HER2 domain I  
680 (orange), H<sub>2</sub>Mab-119 Fab (cyan), and their complex after mixing at 1.5:1 molar ratio (magenta) were  
681 subjected to SEC analysis on Superdex 200 Increase 10/300 GL column. (D) Amino-acid sequence of  
682 the HER2 domain I. Residues in contact with the H<sub>2</sub>Mab-119 (within 4 Å) in the crystal structure  
683 (shown in Figure 3C) are colored in magenta.

684

685 **Figure S3. Flow cytometric analysis of DTT-treated HEK293T cells stained with various anti-  
686 HER2 antibodies.** HEK293T cells were cultured in DMEM/FBS containing 1 mM DTT for 1 or 24  
687 hours and then stained with H<sub>2</sub>Mab-19, H<sub>2</sub>Mab-181, H<sub>2</sub>Mab-41, trastuzumab, or buffer control (gray  
688 histogram), followed by flow cytometry analysis using Alexa Fluor 488-labeled secondary antibodies.  
689 The epitope of each antibody is given below the antibody name.

690

691 **Figure S4. Flow cytometry using H<sub>2</sub>Mab-214-mG<sub>2a</sub>-f and H<sub>2</sub>Mab-119-mG<sub>2a</sub>-f.** (A) A core-fucose-  
692 deficient mouse IgG<sub>2a</sub> mAbs, H<sub>2</sub>Mab-214-mG<sub>2a</sub>-f and H<sub>2</sub>Mab-119-mG<sub>2a</sub>-f were produced from  
693 H<sub>2</sub>Mab-214 (mouse IgG<sub>1</sub>) and H<sub>2</sub>Mab-119 (mouse IgG<sub>1</sub>). (B) BT-474 and MDA-MB-468 cells were  
694 treated with 10  $\mu$ g/ml of H<sub>2</sub>Mab-214-mG<sub>2a</sub>-f, H<sub>2</sub>Mab-119-mG<sub>2a</sub>-f, 281-mG<sub>2a</sub>-f, or buffer control,  
695 followed by Alexa Fluor 488-conjugated anti-mouse IgG. The black line represents the negative  
696 control (blocking buffer).

697

698 **Figure S5. Antitumor activity of H<sub>2</sub>Mab-119-mG<sub>2a</sub>-f and H<sub>2</sub>Mab-214-mG<sub>2a</sub>-f against MDA-MB-  
699 468 xenograft.** (A) MDA-MB-468 cells ( $5 \times 10^6$  cells) were subcutaneously injected into BALB/c  
700 nude mice. On day 7, 100  $\mu$ g of H<sub>2</sub>Mab-119-mG<sub>2a</sub>-f, H<sub>2</sub>Mab-214-mG<sub>2a</sub>-f, control normal mouse IgG

701 or 281-mG<sub>2a</sub>-f were injected intraperitoneally into mice. Additional antibodies were injected on days  
702 14 and 19. The tumor volume was measured on days 7, 12, 14, 19, 22, and 26 after the inoculation of  
703 MDA-MB-468. Values are presented as the mean  $\pm$  SEM. n.s., not significant (B) Tumor weight (day  
704 26) was measured from excised MDA-MB-468 xenograft tumors. Values are presented as the mean  $\pm$   
705 SEM. n.s., not significant. (C) Appearance of MDA-MB-468 xenograft tumors from the H<sub>2</sub>Mab-119-  
706 mG<sub>2a</sub>-f, H<sub>2</sub>Mab-214-mG<sub>2a</sub>-f, control normal mouse IgG and 281-mG<sub>2a</sub>-f-treated mice on day 26 (scale  
707 bar, 1 cm). (D) Mice weight in H<sub>2</sub>Mab-119-mG<sub>2a</sub>-f, H<sub>2</sub>Mab-214-mG<sub>2a</sub>-f, control normal mouse IgG  
708 and 281-mG<sub>2a</sub>-f-treated groups. n.s., not significant.

709

710 **Figure S6. Body appearance of mice.** Body appearance of BT-474 (A) and MDA-MB-468 (B)  
711 xenograft-bearing mice on day 26. Scale bar, 1 cm.

712

713 **Table S1 Data collection and refinement statistics**

	H <sub>2</sub> Mab-214 Fv-clasp/epitope peptide complex (PDB: 8jyq)	H <sub>2</sub> Mab-119 Fab/HER2 domain I complex (PDB: 8jyr)
<b>Data collection</b>		
Space group	<i>P</i> 2 <sub>1</sub>	<i>P</i> 2 <sub>1</sub>
Cell dimensions		
<i>a, b, c</i> (Å)	73.14, 62.79, 78.12	53.98, 112.29, 60.54
β (°)	94.42	90.76
Resolution (Å)	47.58 - 1.75 (1.85 - 1.75) <sup>a</sup>	48.65 - 1.69 (1.80 - 1.69)
<i>R</i> <sub>sym</sub> (%)	5.2 (96.1)	6.6 (91.2)
<i>I</i> / $\sigma$ <i>I</i>	10.95 (1.05)	9.46 (1.35)
CC1/2 (%)	99.8 (70.8)	99.7 (69.4)
Completeness (%)	98.6 (97.2)	99.1 (97.9)
Redundancy	3.9 (3.8)	3.5 (3.6)
<b>Refinement</b>		
Resolution (Å)	36.46 – 1.75	40.02 – 1.69
No. reflections	70,773	79,290
<i>R</i> <sub>work</sub> / <i>R</i> <sub>free</sub> (%)	19.6 / 23.3	17.3 / 20.9
No. atoms		
Protein	5,261	4,743
Peptide	138	14
Water	193	475
<i>B</i> -factors		
Protein	54.2	37.7
Peptide	52.7	-
Carbohydrate	-	68.1
Water	47.8	42.5
R.m.s. deviations		
Bond lengths (Å)	0.006	0.015
Bond angles (°)	0.881	1.324

714 <sup>a</sup>Values in parentheses are statistics of the highest-resolution shell.

715

716 **References**

- 717 1. Yarden, Y., and Sliwkowski, M.X. (2001). Untangling the ErbB signalling network. *Nat Rev Mol*  
718 *Cell Biol* 2, 127-137. 10.1038/35052073.
- 719 2. Cho, H.S., and Leahy, D.J. (2002). Structure of the extracellular region of HER3 reveals an  
720 interdomain tether. *Science* 297, 1330-1333. 10.1126/science.1074611.
- 721 3. Ferguson, K.M., Berger, M.B., Mendrola, J.M., Cho, H.S., Leahy, D.J., and Lemmon, M.A. (2003).  
722 EGF activates its receptor by removing interactions that autoinhibit ectodomain dimerization. *Mol*  
723 *Cell* 11, 507-517. 10.1016/s1097-2765(03)00047-9.
- 724 4. Bouyain, S., Longo, P.A., Li, S., Ferguson, K.M., and Leahy, D.J. (2005). The extracellular region  
725 of ErbB4 adopts a tethered conformation in the absence of ligand. *Proc Natl Acad Sci U S A* 102,  
726 15024-15029. 10.1073/pnas.0507591102.
- 727 5. Ogiso, H., Ishitani, R., Nureki, O., Fukai, S., Yamanaka, M., Kim, J.H., Saito, K., Sakamoto, A.,  
728 Inoue, M., Shirouzu, M., and Yokoyama, S. (2002). Crystal structure of the complex of human  
729 epidermal growth factor and receptor extracellular domains. *Cell* 110, 775-787. 10.1016/s0092-  
730 8674(02)00963-7.
- 731 6. Garrett, T.P., McKern, N.M., Lou, M., Elleman, T.C., Adams, T.E., Lovrecz, G.O., Zhu, H.J.,  
732 Walker, F., Frenkel, M.J., Hoyne, P.A., et al. (2002). Crystal structure of a truncated epidermal  
733 growth factor receptor extracellular domain bound to transforming growth factor alpha. *Cell* 110,  
734 763-773. 10.1016/s0092-8674(02)00940-6.
- 735 7. Liu, P., Cleveland, T.E.t., Bouyain, S., Byrne, P.O., Longo, P.A., and Leahy, D.J. (2012). A single  
736 ligand is sufficient to activate EGFR dimers. *Proc Natl Acad Sci U S A* 109, 10861-10866.  
737 10.1073/pnas.120114109.
- 738 8. Cho, H.S., Mason, K., Ramyar, K.X., Stanley, A.M., Gabelli, S.B., Denney, D.W., Jr., and Leahy,  
739 D.J. (2003). Structure of the extracellular region of HER2 alone and in complex with the Herceptin  
740 Fab. *Nature* 421, 756-760. 10.1038/nature01392.
- 741 9. Diwanji, D., Trenker, R., Thaker, T.M., Wang, F., Agard, D.A., Verba, K.A., and Jura, N. (2021).  
742 Structures of the HER2-HER3-NRG1beta complex reveal a dynamic dimer interface. *Nature* 600,  
743 339-343. 10.1038/s41586-021-04084-z.
- 744 10. Citri, A., and Yarden, Y. (2006). EGF-ERBB signalling: towards the systems level. *Nat Rev Mol*  
745 *Cell Biol* 7, 505-516. 10.1038/nrm1962.
- 746 11. Rimawi, M.F., Schiff, R., and Osborne, C.K. (2015). Targeting HER2 for the treatment of breast  
747 cancer. *Annu Rev Med* 66, 111-128. 10.1146/annurev-med-042513-015127.
- 748 12. Slamon, D.J., Clark, G.M., Wong, S.G., Levin, W.J., Ullrich, A., and McGuire, W.L. (1987).  
749 Human breast cancer: correlation of relapse and survival with amplification of the HER-2/neu  
750 oncogene. *Science* 235, 177-182. 10.1126/science.3798106.
- 751 13. Van Cutsem, E., Bang, Y.J., Feng-Yi, F., Xu, J.M., Lee, K.W., Jiao, S.C., Chong, J.L., López-

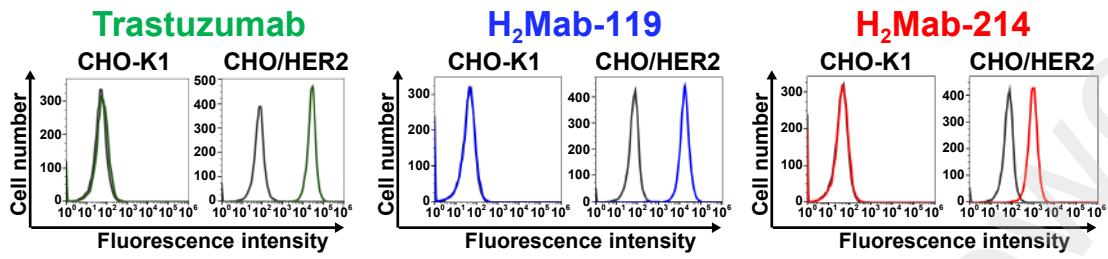
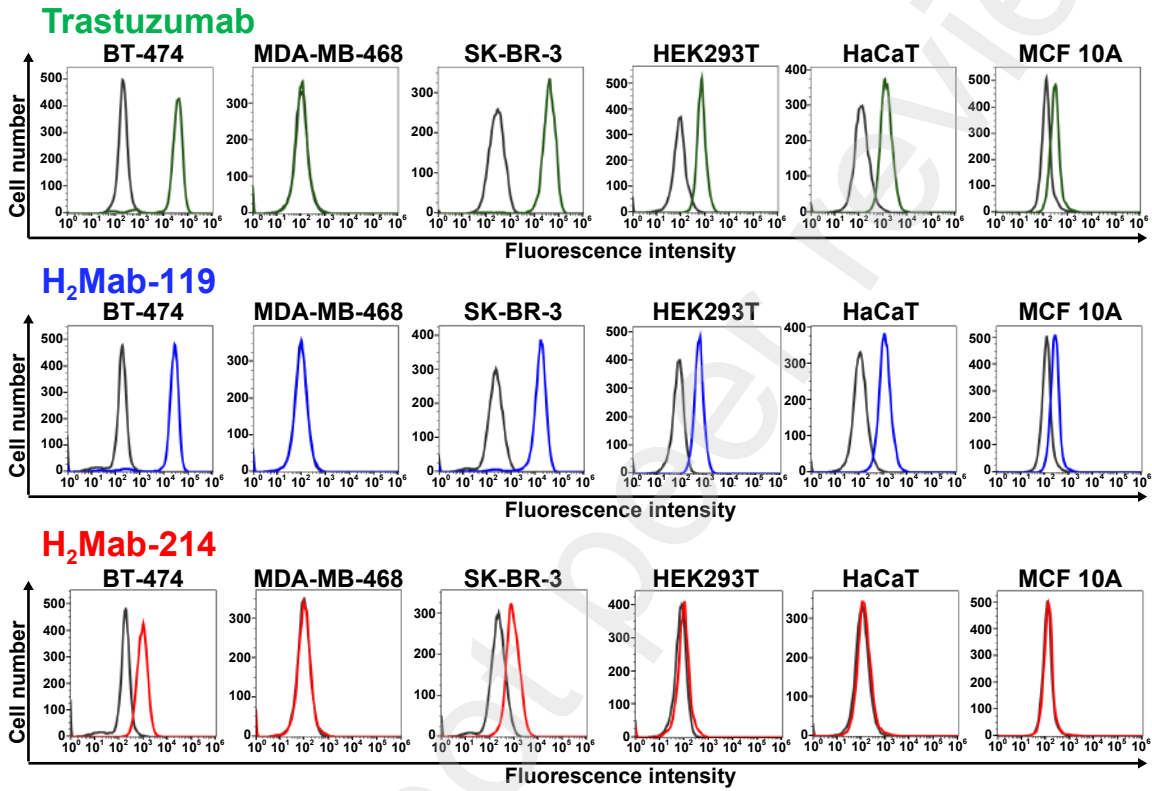
- 752 Sanchez, R.I., Price, T., Gladkov, O., et al. (2015). HER2 screening data from ToGA: targeting  
753 HER2 in gastric and gastroesophageal junction cancer. *Gastric Cancer* 18, 476-484.  
754 10.1007/s10120-014-0402-y.
- 755 14. Tsao, L.C., Force, J., and Hartman, Z.C. (2021). Mechanisms of Therapeutic Antitumor  
756 Monoclonal Antibodies. *Cancer Res* 81, 4641-4651. 10.1158/0008-5472.Can-21-1109.
- 757 15. Essadi, I., Benbrahim, Z., Kaakoua, M., Reverdy, T., Corbaux, P., and Freyer, G. (2023). HER2-  
758 Positive Metastatic Breast Cancer: Available Treatments and Current Developments. *Cancers*  
759 (Basel) 15. 10.3390/cancers15061738.
- 760 16. Slamon, D.J., Leyland-Jones, B., Shak, S., Fuchs, H., Paton, V., Bajamonde, A., Fleming, T.,  
761 Eiermann, W., Wolter, J., Pegram, M., et al. (2001). Use of chemotherapy plus a monoclonal  
762 antibody against HER2 for metastatic breast cancer that overexpresses HER2. *N Engl J Med* 344,  
763 783-792. 10.1056/nejm200103153441101.
- 764 17. Bang, Y.J., Van Cutsem, E., Feyereislova, A., Chung, H.C., Shen, L., Sawaki, A., Lordick, F.,  
765 Ohtsu, A., Omuro, Y., Satoh, T., et al. (2010). Trastuzumab in combination with chemotherapy  
766 versus chemotherapy alone for treatment of HER2-positive advanced gastric or gastro-  
767 oesophageal junction cancer (ToGA): a phase 3, open-label, randomised controlled trial. *Lancet*  
768 376, 687-697. 10.1016/s0140-6736(10)61121-x.
- 769 18. Musolino, A., Gradishar, W.J., Rugo, H.S., Nordstrom, J.L., Rock, E.P., Arnaldez, F., and Pegram,  
770 M.D. (2022). Role of Fc $\gamma$  receptors in HER2-targeted breast cancer therapy. *J Immunother Cancer*  
771 10. 10.1136/jitc-2021-003171.
- 772 19. Nordstrom, J.L., Gorlatov, S., Zhang, W., Yang, Y., Huang, L., Burke, S., Li, H., Ciccarone, V.,  
773 Zhang, T., Stavenhagen, J., et al. (2011). Anti-tumor activity and toxicokinetics analysis of  
774 MGAH22, an anti-HER2 monoclonal antibody with enhanced Fc $\gamma$  receptor binding properties.  
775 *Breast Cancer Res* 13, R123. 10.1186/bcr3069.
- 776 20. McAndrew, N.P. (2022). Updates on targeting human epidermal growth factor receptor 2-positive  
777 breast cancer: what's to know in 2021. *Curr Opin Obstet Gynecol* 34, 41-45.  
778 10.1097/gco.0000000000000762.
- 779 21. Rugo, H.S., Im, S.A., Cardoso, F., Cortés, J., Curigliano, G., Musolino, A., Pegram, M.D., Wright,  
780 G.S., Saura, C., Escrivá-de-Romaní, S., et al. (2021). Efficacy of Margetuximab vs Trastuzumab  
781 in Patients With Pretreated ERBB2-Positive Advanced Breast Cancer: A Phase 3 Randomized  
782 Clinical Trial. *JAMA Oncol* 7, 573-584. 10.1001/jamaoncol.2020.7932.
- 783 22. Golay, J., and Taylor, R.P. (2020). The Role of Complement in the Mechanism of Action of  
784 Therapeutic Anti-Cancer mAbs. *Antibodies (Basel)* 9. 10.3390/antib9040058.
- 785 23. Reis, E.S., Mastellos, D.C., Ricklin, D., Mantovani, A., and Lambris, J.D. (2018). Complement in  
786 cancer: untangling an intricate relationship. *Nat Rev Immunol* 18, 5-18. 10.1038/nri.2017.97.
- 787 24. Gala, K., and Chandarlapaty, S. (2014). Molecular pathways: HER3 targeted therapy. *Clin Cancer*

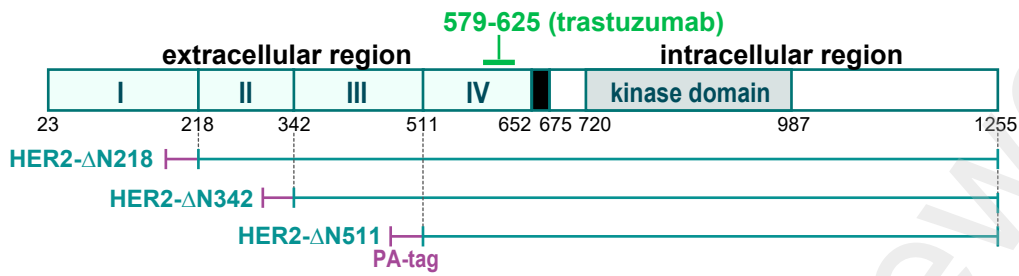
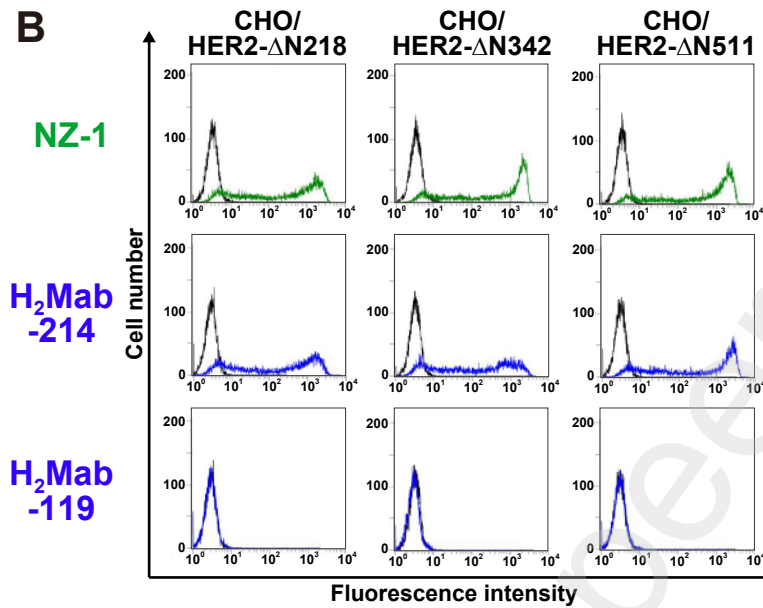
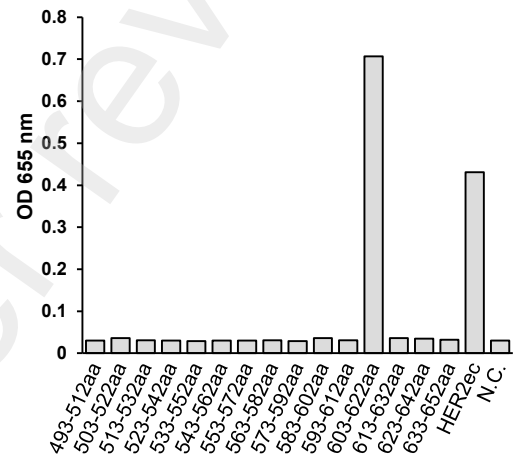
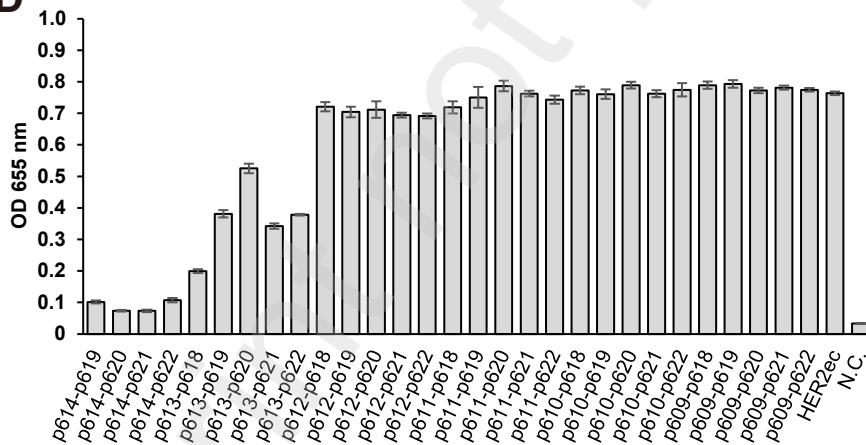
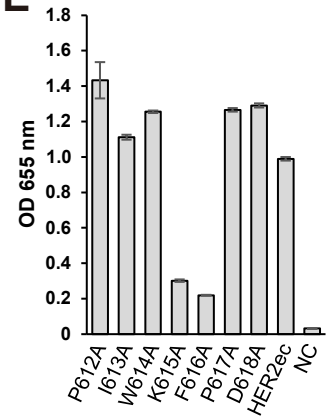
- 788 Res 20, 1410-1416. 10.1158/1078-0432.CCR-13-1549.
- 789 25. Franklin, M.C., Carey, K.D., Vajdos, F.F., Leahy, D.J., de Vos, A.M., and Sliwkowski, M.X.  
790 (2004). Insights into ErbB signaling from the structure of the ErbB2-pertuzumab complex. *Cancer*  
791 *Cell* 5, 317-328. 10.1016/s1535-6108(04)00083-2.
- 792 26. Badache, A., and Hynes, N.E. (2004). A new therapeutic antibody masks ErbB2 to its partners.  
793 *Cancer Cell* 5, 299-301. 10.1016/s1535-6108(04)00088-1.
- 794 27. Swain, S.M., Baselga, J., Kim, S.B., Ro, J., Semiglazov, V., Campone, M., Ciruelos, E., Ferrero,  
795 J.M., Schneeweiss, A., Heeson, S., et al. (2015). Pertuzumab, trastuzumab, and docetaxel in  
796 HER2-positive metastatic breast cancer. *N Engl J Med* 372, 724-734. 10.1056/NEJMoa1413513.
- 797 28. Copeland-Halperin, R.S., Liu, J.E., and Yu, A.F. (2019). Cardiotoxicity of HER2-targeted  
798 therapies. *Curr Opin Cardiol* 34, 451-458. 10.1097/hco.0000000000000637.
- 799 29. Lee, K.F., Simon, H., Chen, H., Bates, B., Hung, M.C., and Hauser, C. (1995). Requirement for  
800 neuregulin receptor erbB2 in neural and cardiac development. *Nature* 378, 394-398.  
801 10.1038/378394a0.
- 802 30. Crone, S.A., Zhao, Y.Y., Fan, L., Gu, Y., Minamisawa, S., Liu, Y., Peterson, K.L., Chen, J., Kahn,  
803 R., Condorelli, G., et al. (2002). ErbB2 is essential in the prevention of dilated cardiomyopathy.  
804 *Nat Med* 8, 459-465. 10.1038/nm0502-459.
- 805 31. Wang, D., Eraslan, B., Wieland, T., Hallstrom, B., Hopf, T., Zolg, D.P., Zecha, J., Asplund, A.,  
806 Li, L.H., Meng, C., et al. (2019). A deep proteome and transcriptome abundance atlas of 29 healthy  
807 human tissues. *Mol Syst Biol* 15, e8503. 10.15252/msb.20188503.
- 808 32. Kato, Y., and Kaneko, M.K. (2014). A cancer-specific monoclonal antibody recognizes the  
809 aberrantly glycosylated podoplanin. *Sci Rep* 4, 5924. 10.1038/srep05924.
- 810 33. Yamada, S., Ogasawara, S., Kaneko, M.K., and Kato, Y. (2017). LpMab-23: A Cancer-Specific  
811 Monoclonal Antibody Against Human Podoplanin. *Monoclon Antib Immunodiagn Immunother*  
812 36, 72-76. 10.1089/mab.2017.0001.
- 813 34. Kaneko, M.K., Ohishi, T., Kawada, M., and Kato, Y. (2020). A cancer-specific anti-podocalyxin  
814 monoclonal antibody (60-mG(2a)-f) exerts antitumor effects in mouse xenograft models of  
815 pancreatic carcinoma. *Biochem Biophys Rep* 24, 100826. 10.1016/j.bbrep.2020.100826.
- 816 35. Suzuki, H., Kaneko, M.K., and Kato, Y. (2022). Roles of Podoplanin in Malignant Progression of  
817 Tumor. *Cells* 11. 10.3390/cells11030575.
- 818 36. Yamada, S., Itai, S., Nakamura, T., Chang, Y.W., Harada, H., Suzuki, H., Kaneko, M.K., and  
819 Kato, Y. (2017). Establishment of H(2)Mab-119, an Anti-Human Epidermal Growth Factor  
820 Receptor 2 Monoclonal Antibody, Against Pancreatic Cancer. *Monoclon Antib Immunodiagn*  
821 *Immunother* 36, 287-290. 10.1089/mab.2017.0050.
- 822 37. Kumar, R., Shepard, H.M., and Mendelsohn, J. (1991). Regulation of phosphorylation of the c-  
823 erbB-2/HER2 gene product by a monoclonal antibody and serum growth factor(s) in human

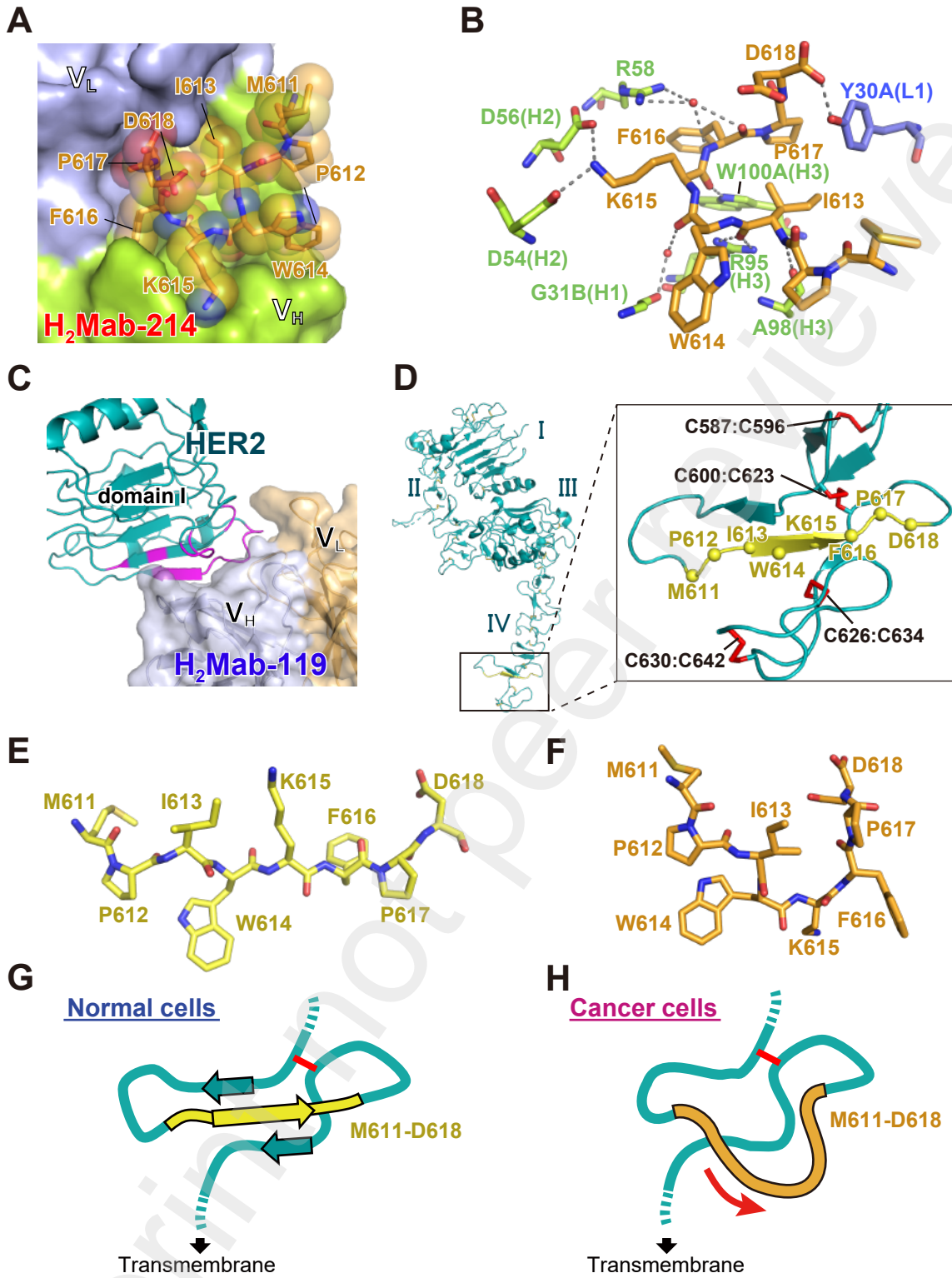
- 824 mammary carcinoma cells. *Mol Cell Biol* *11*, 979-986. 10.1128/mcb.11.2.979-986.1991.
- 825 38. Roetger, A., Merschjann, A., Dittmar, T., Jackisch, C., Barnekow, A., and Brandt, B. (1998).  
826 Selection of potentially metastatic subpopulations expressing c-erbB-2 from breast cancer tissue  
827 by use of an extravasation model. *Am J Pathol* *153*, 1797-1806. 10.1016/S0002-9440(10)65694-  
828 5.
- 829 39. Arimori, T., Kitago, Y., Umitsu, M., Fujii, Y., Asaki, R., Tamura-Kawakami, K., and Takagi, J.  
830 (2017). Fv-clasp: An Artificially Designed Small Antibody Fragment with Improved Production  
831 Compatibility, Stability, and Crystallizability. *Structure* *25*, 1611-1622 e1614.  
832 10.1016/j.str.2017.08.011.
- 833 40. Takei, J., Kaneko, M.K., Ohishi, T., Kawada, M., Harada, H., and Kato, Y. (2020). H(2)Mab-19,  
834 an anti-human epidermal growth factor receptor 2 monoclonal antibody exerts antitumor activity  
835 in mouse oral cancer xenografts. *Exp Ther Med* *20*, 846-853. 10.3892/etm.2020.8765.
- 836 41. Asano, T., Takei, J., Suzuki, H., Kaneko, M.K., and Kato, Y. (2021). Epitope Mapping of an Anti-  
837 HER2 Monoclonal Antibody (H(2)Mab-181) Using Enzyme-Linked Immunosorbent Assay.  
838 *Monoclon Antib Immunodiagn Immunother* *40*, 255-260. 10.1089/mab.2021.0029.
- 839 42. Kato, Y., Ohishi, T., Yamada, S., Itai, S., Takei, J., Sano, M., Nakamura, T., Harada, H., Kawada,  
840 M., and Kaneko, M.K. (2019). Anti-Human Epidermal Growth Factor Receptor 2 Monoclonal  
841 Antibody H(2)Mab-41 Exerts Antitumor Activity in a Mouse Xenograft Model of Colon Cancer.  
842 *Monoclon Antib Immunodiagn Immunother* *38*, 157-161. 10.1089/mab.2019.0017.
- 843 43. Li, G., Suzuki, H., Ohishi, T., Asano, T., Tanaka, T., Yanaka, M., Nakamura, T., Yoshikawa, T.,  
844 Kawada, M., Kaneko, M.K., and Kato, Y. (2023). Antitumor activities of a defucosylated  
845 anti-EpCAM monoclonal antibody in colorectal carcinoma xenograft models. *Int J Mol Med* *51*.  
846 10.3892/ijmm.2023.5221.
- 847 44. Nanamiya, R., Takei, J., Ohishi, T., Asano, T., Tanaka, T., Sano, M., Nakamura, T., Yanaka, M.,  
848 Handa, S., Tateyama, N., et al. (2022). Defucosylated Anti-Epidermal Growth Factor Receptor  
849 Monoclonal Antibody (134-mG(2a)-f) Exerts Antitumor Activities in Mouse Xenograft Models  
850 of Canine Osteosarcoma. *Monoclon Antib Immunodiagn Immunother* *41*, 1-7.  
851 10.1089/mab.2021.0036.
- 852 45. Kawabata, H., Suzuki, H., Ohishi, T., Kawada, M., Kaneko, M.K., and Kato, Y. (2022). A  
853 Defucosylated Mouse Anti-CD10 Monoclonal Antibody (31-mG(2a)-f) Exerts Antitumor Activity  
854 in a Mouse Xenograft Model of CD10-Overexpressed Tumors. *Monoclon Antib Immunodiagn*  
855 *Immunother* *41*, 59-66. 10.1089/mab.2021.0048.
- 856 46. Kawabata, H., Ohishi, T., Suzuki, H., Asano, T., Kawada, M., Suzuki, H., Kaneko, M.K., and  
857 Kato, Y. (2022). A Defucosylated Mouse Anti-CD10 Monoclonal Antibody (31-mG(2a)-f) Exerts  
858 Antitumor Activity in a Mouse Xenograft Model of Renal Cell Cancers. *Monoclon Antib*  
859 *Immunodiagn Immunother*. 10.1089/mab.2021.0049.

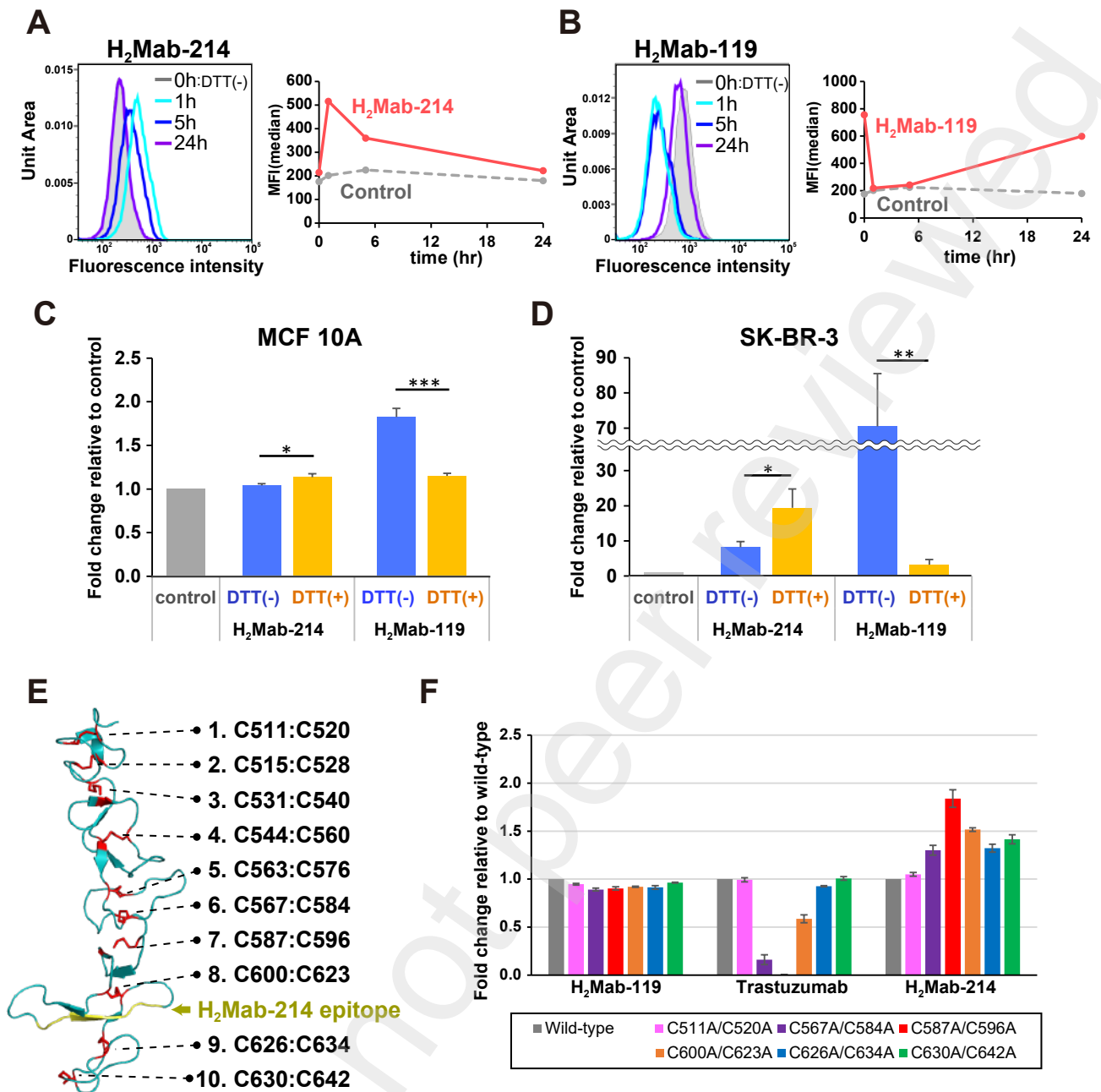
- 860 47. Asano, T., Tanaka, T., Suzuki, H., Li, G., Ohishi, T., Kawada, M., Yoshikawa, T., Kaneko, M.K.,  
861 and Kato, Y. (2022). A Defucosylated Anti-EpCAM Monoclonal Antibody (EpMab-37-mG(2a)-  
862 f) Exerts Antitumor Activity in Xenograft Model. *Antibodies (Basel) 11*. 10.3390/antib11040074.
- 863 48. Tateyama, N., Nanamiya, R., Ohishi, T., Takei, J., Nakamura, T., Yanaka, M., Hosono, H., Saito,  
864 M., Asano, T., Tanaka, T., et al. (2021). Defucosylated Anti-Epidermal Growth Factor Receptor  
865 Monoclonal Antibody 134-mG(2a)-f Exerts Antitumor Activities in Mouse Xenograft Models of  
866 Dog Epidermal Growth Factor Receptor-Overexpressed Cells. *Monoclon Antib Immunodiagn*  
867 *Immunother 40*, 177-183. 10.1089/mab.2021.0022.
- 868 49. Takei, J., Ohishi, T., Kaneko, M.K., Harada, H., Kawada, M., and Kato, Y. (2020). A  
869 defucosylated anti-PD-L1 monoclonal antibody 13-mG(2a)-f exerts antitumor effects in mouse  
870 xenograft models of oral squamous cell carcinoma. *Biochem Biophys Rep 24*, 100801.  
871 10.1016/j.bbrep.2020.100801.
- 872 50. Takei, J., Kaneko, M.K., Ohishi, T., Hosono, H., Nakamura, T., Yanaka, M., Sano, M., Asano, T.,  
873 Sayama, Y., Kawada, M., et al. (2020). A defucosylated antiCD44 monoclonal antibody 5mG2af  
874 exerts antitumor effects in mouse xenograft models of oral squamous cell carcinoma. *Oncol Rep*  
875 *44*, 1949-1960. 10.3892/or.2020.7735.
- 876 51. Maadi, H., Soheilifar, M.H., Choi, W.S., Moshtaghian, A., and Wang, Z. (2021). Trastuzumab  
877 Mechanism of Action; 20 Years of Research to Unravel a Dilemma. *Cancers (Basel) 13*.  
878 10.3390/cancers13143540.
- 879 52. Lu, R.M., Hwang, Y.C., Liu, I.J., Lee, C.C., Tsai, H.Z., Li, H.J., and Wu, H.C. (2020).  
880 Development of therapeutic antibodies for the treatment of diseases. *J Biomed Sci 27*, 1.  
881 10.1186/s12929-019-0592-z.
- 882 53. Scott, A.M., Lee, F.T., Tebbutt, N., Herbertson, R., Gill, S.S., Liu, Z., Skrinos, E., Murone, C.,  
883 Saunder, T.H., Chappell, B., et al. (2007). A phase I clinical trial with monoclonal antibody ch806  
884 targeting transitional state and mutant epidermal growth factor receptors. *Proc Natl Acad Sci U S*  
885 *A 104*, 4071-4076. 10.1073/pnas.0611693104.
- 886 54. Hosen, N., Matsunaga, Y., Hasegawa, K., Matsuno, H., Nakamura, Y., Makita, M., Watanabe, K.,  
887 Yoshida, M., Satoh, K., Morimoto, S., et al. (2017). The activated conformation of integrin beta7  
888 is a novel multiple myeloma-specific target for car T cell therapy. *Nat. Med. 23*, 1436-1443.  
889 10.1038/nm.4431. .
- 890 55. Garrett, T.P., Burgess, A.W., Gan, H.K., Luwor, R.B., Cartwright, G., Walker, F., Orchard, S.G.,  
891 Clayton, A.H., Nice, E.C., Rothacker, J., et al. (2009). Antibodies specifically targeting a locally  
892 misfolded region of tumor associated EGFR. *Proc Natl Acad Sci U S A 106*, 5082-5087.  
893 10.1073/pnas.0811559106.
- 894 56. Oakes, S.A. (2020). Endoplasmic Reticulum Stress Signaling in Cancer Cells. *Am J Pathol 190*,  
895 934-946. 10.1016/j.ajpath.2020.01.010.

- 896 57. Powell, L.E., and Foster, P.A. (2021). Protein disulphide isomerase inhibition as a potential cancer  
897 therapeutic strategy. *Cancer Med* 10, 2812-2825. 10.1002/cam4.3836.
- 898 58. Kato, Y., Kaneko, M.K., Kuno, A., Uchiyama, N., Amano, K., Chiba, Y., Hasegawa, Y.,  
899 Hirabayashi, J., Narimatsu, H., Mishima, K., and Osawa, M. (2006). Inhibition of tumor cell-  
900 induced platelet aggregation using a novel anti-podoplanin antibody reacting with its platelet-  
901 aggregation-stimulating domain. *Biochem Biophys Res Commun* 349, 1301-1307.  
902 10.1016/j.bbrc.2006.08.171.
- 903 59. Suzuki, H., Ohishi, T., Asano, T., Tanaka, T., Saito, M., Mizuno, T., Yoshikawa, T., Kawada, M.,  
904 Kaneko, M.K., and Kato, Y. (2022). Defucosylated mouse-dog chimeric anti-HER2 monoclonal  
905 antibody exerts antitumor activities in mouse xenograft models of canine tumors. *Oncol Rep* 48.  
906 10.3892/or.2022.8366.
- 907 60. Kabsch, W. (2010). *Xds. Acta. Crystallogr. D. Biol. Crystallogr.* 66, 125-132.  
908 10.1107/S0907444909047337.
- 909 61. McCoy, A.J., Grosse-Kunstleve, R.W., Adams, P.D., Winn, M.D., Storoni, L.C., and Read, R.J.  
910 (2007). Phaser crystallographic software. *J. Appl. Cryst.* 40, 658-674.  
911 10.1107/S0021889807021206.
- 912 62. Winn, M.D., Ballard, C.C., Cowtan, K.D., Dodson, E.J., Emsley, P., Evans, P.R., Keegan, R.M.,  
913 Krissinel, E.B., Leslie, A.G., McCoy, A., et al. (2011). Overview of the CCP4 suite and current  
914 developments. *Acta Crystallogr. D Biol. Crystallogr.* 67, 235-242. 10.1107/S0907444910045749.
- 915 63. Emsley, P., Lohkamp, B., Scott, W.G., and Cowtan, K. (2010). Features and development of Coot.  
916 *Acta. Crystallogr. D. Biol. Crystallogr.* 66, 486-501. 10.1107/S0907444910007493.
- 917 64. Adams, P.D., Afonine, P.V., Bunkoczi, G., Chen, V.B., Davis, I.W., Echols, N., Headd, J.J., Hung,  
918 L.W., Kapral, G.J., Grosse-Kunstleve, R.W., et al. (2010). PHENIX: a comprehensive Python-  
919 based system for macromolecular structure solution. *Acta. Crystallogr. D. Biol. Crystallogr.* 66,  
920 213-221. 10.1107/S0907444909052925.
- 921 65. Chen, V.B., Arendall, W.B., Headd, J.J., Keedy, D.A., Immormino, R.M., Kapral, G.J., Murray,  
922 L.W., Richardson, J.S., and Richardson, D.C. (2010). MolProbity: all-atom structure validation  
923 for macromolecular crystallography. *Acta. Crystallogr. D. Biol. Crystallogr.* 66, 12-21.  
924 10.1107/S0907444909042073.  
925

**A****B**

**A****B****C****D****E**





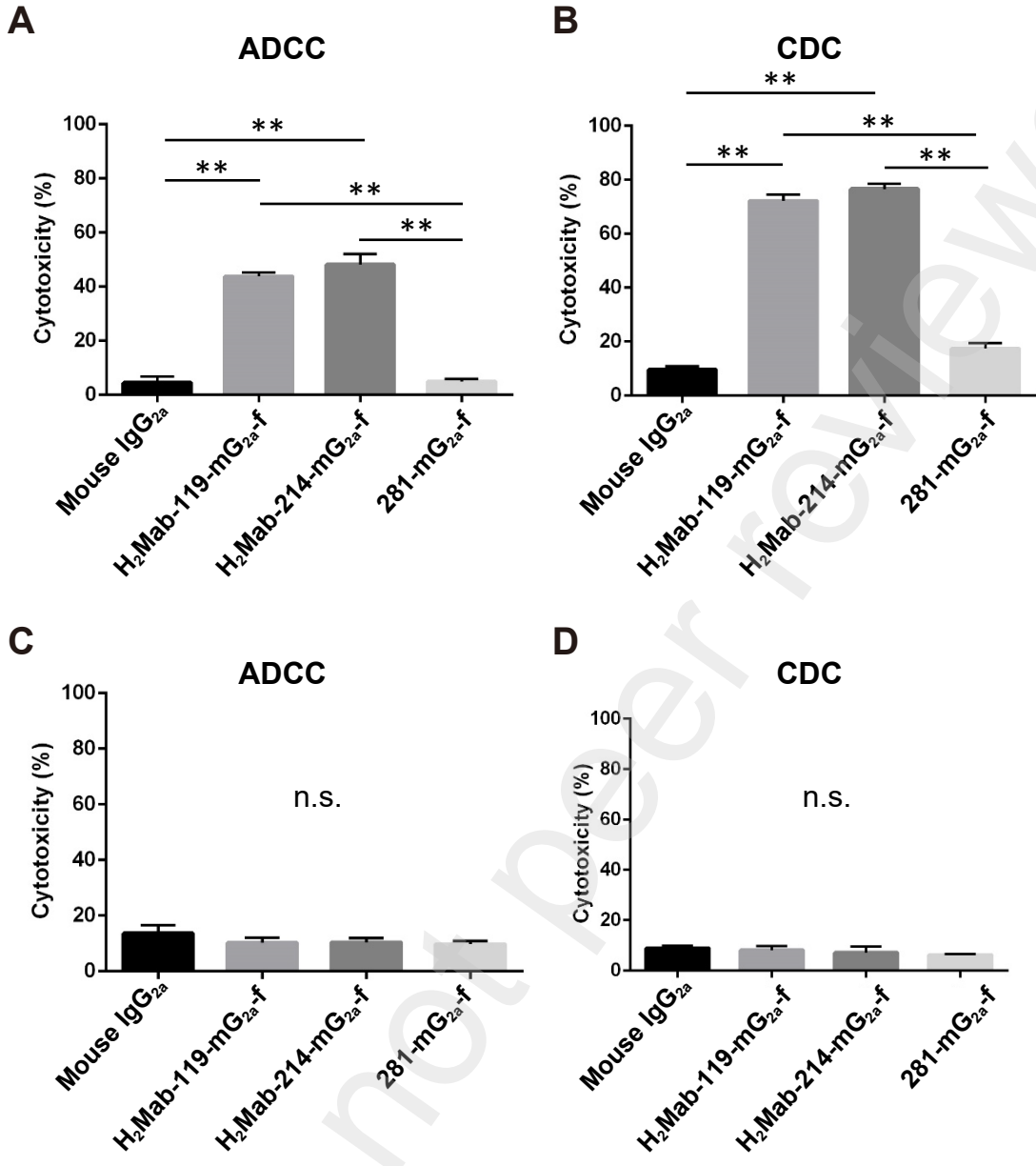


Figure 5

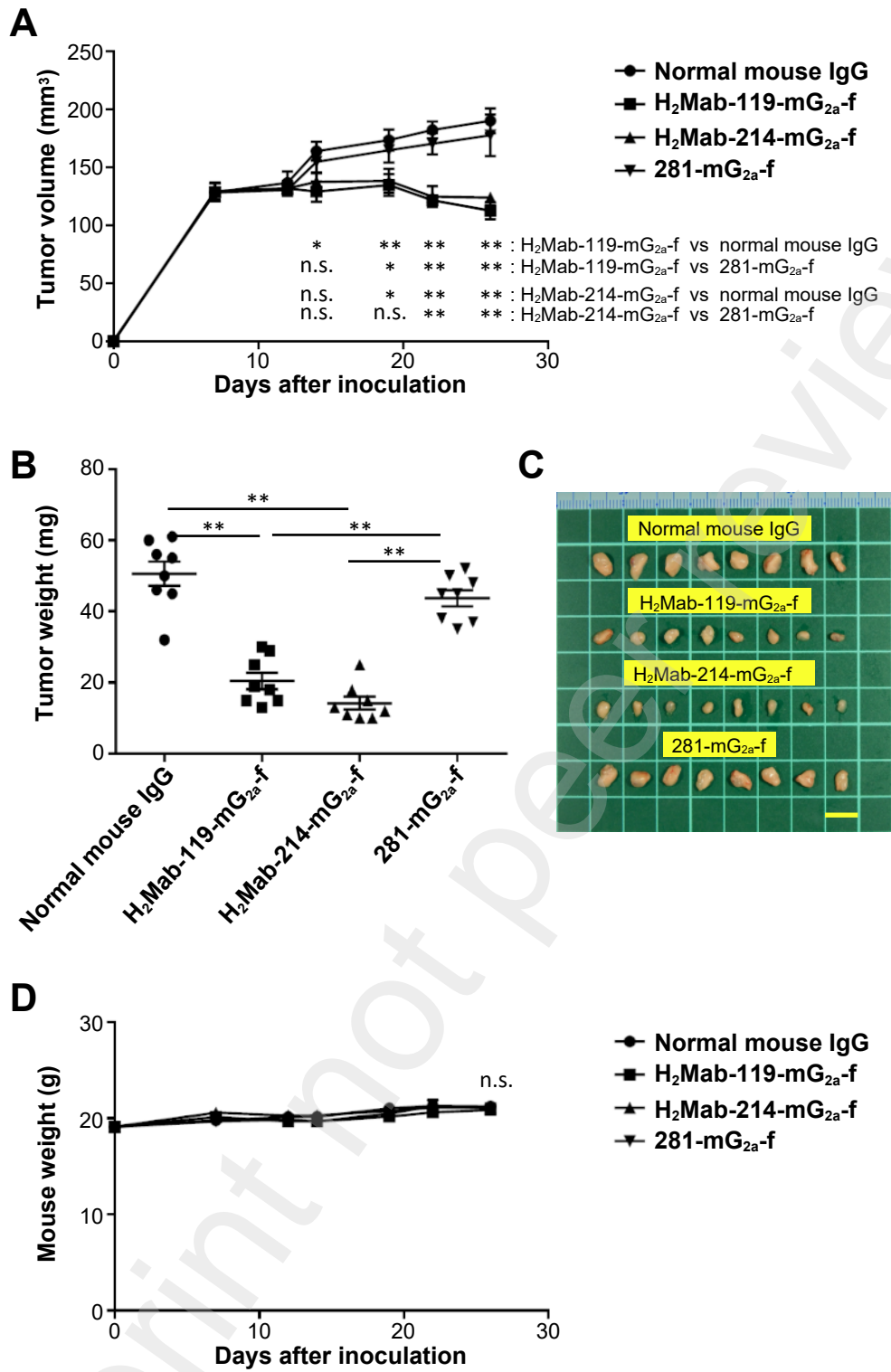
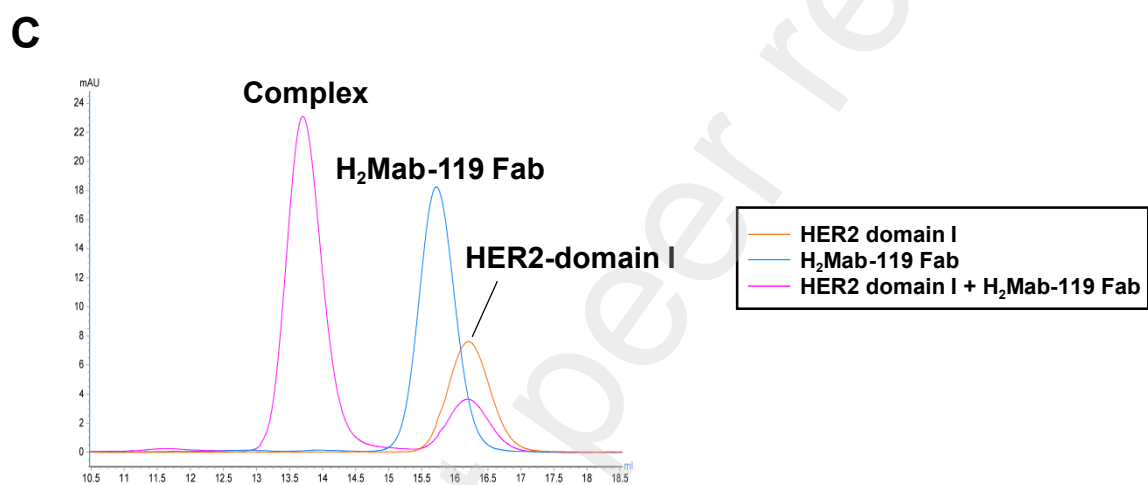
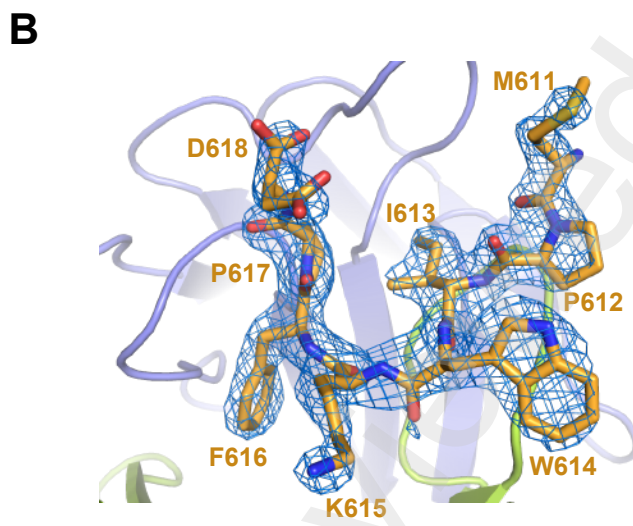
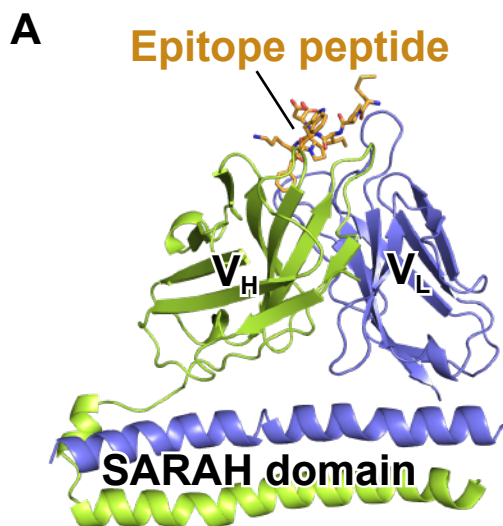


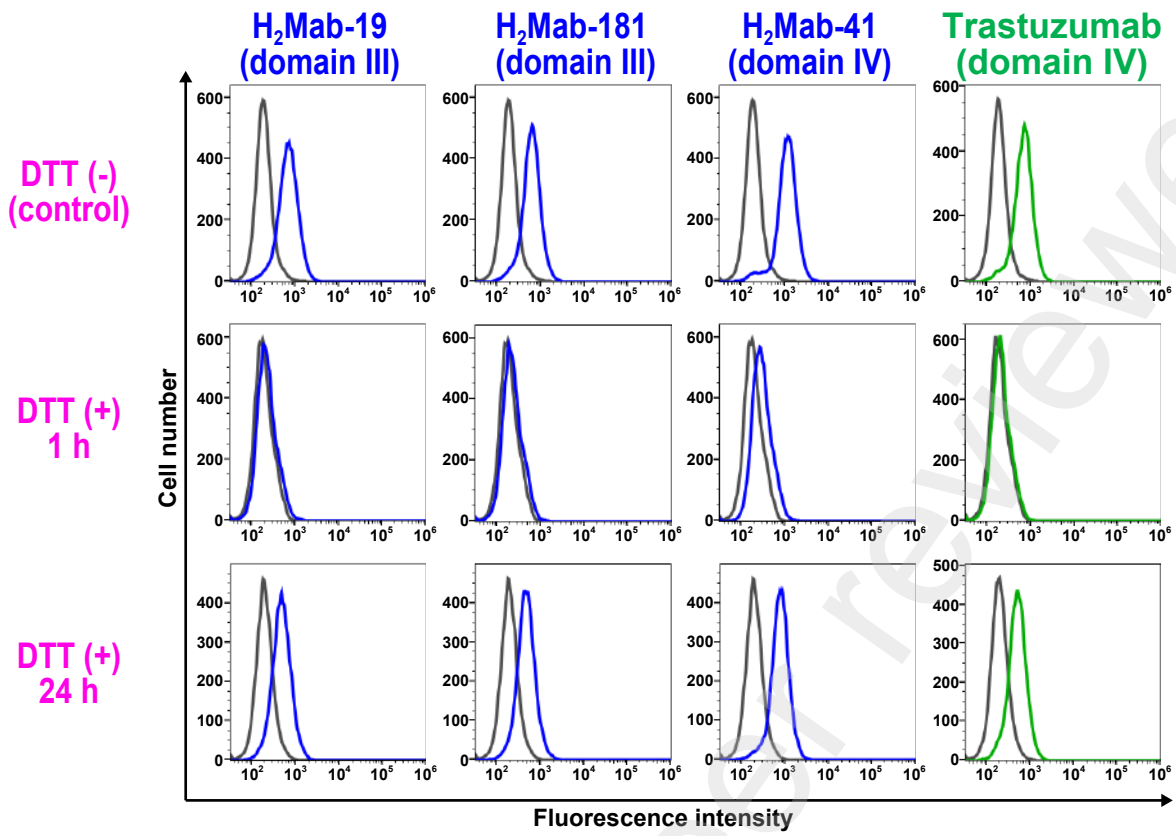
Figure 6

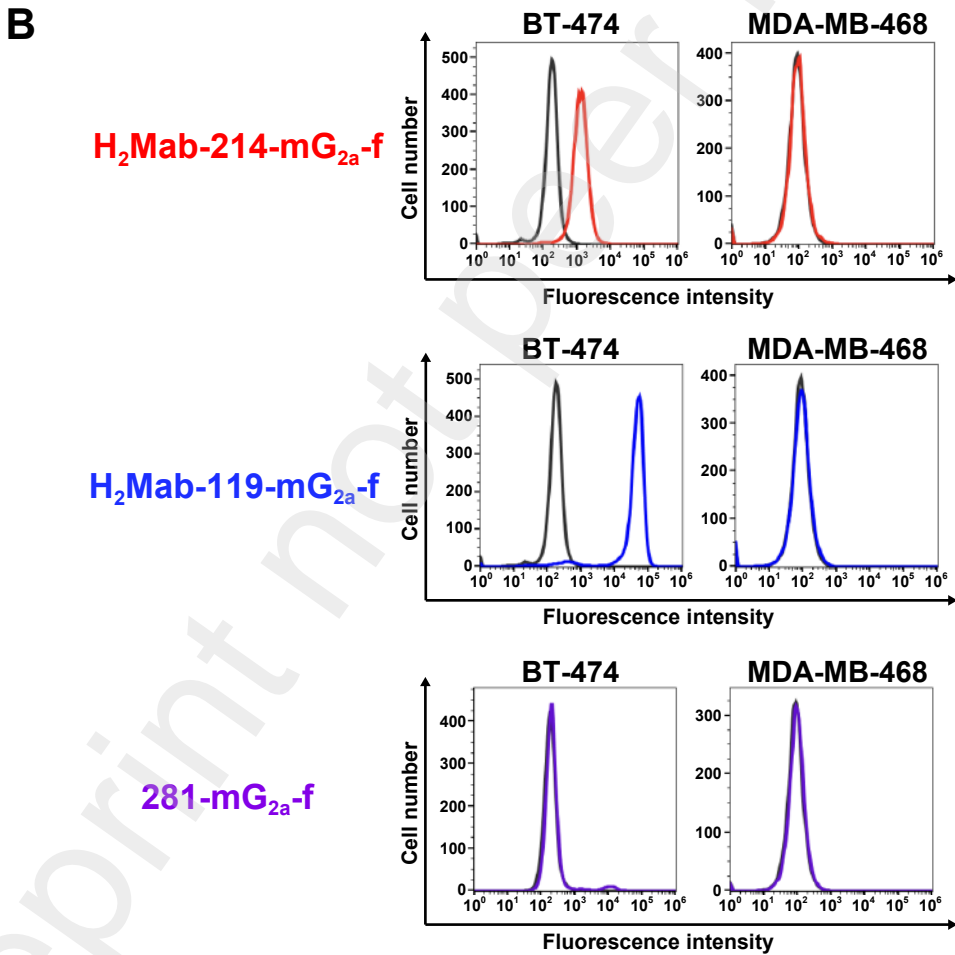
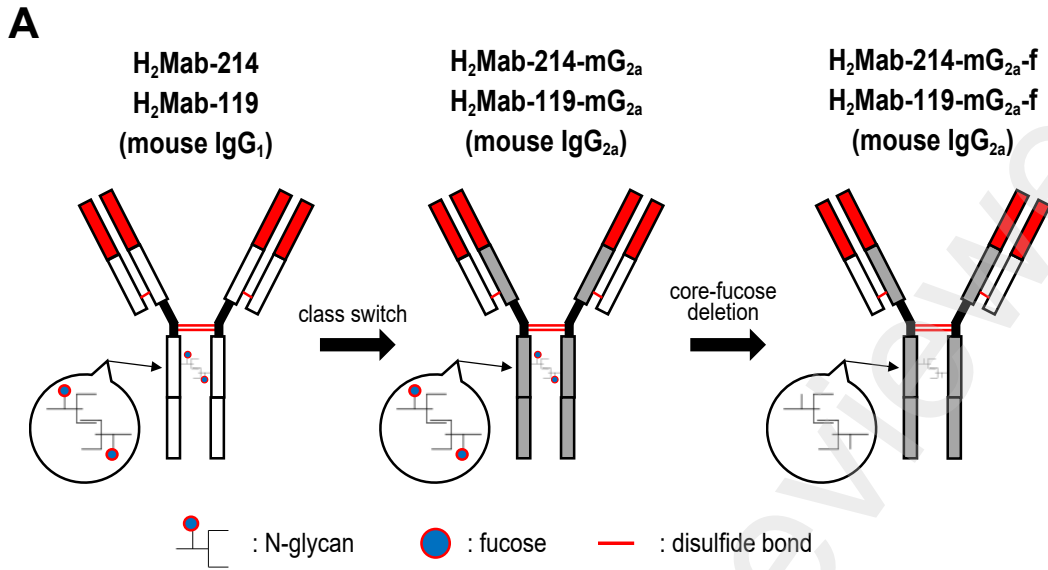


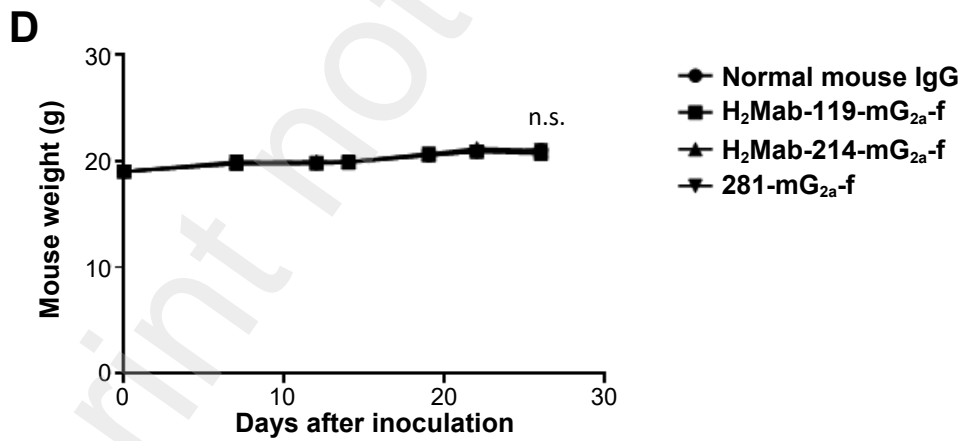
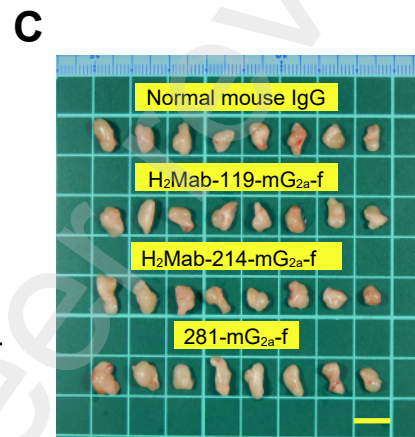
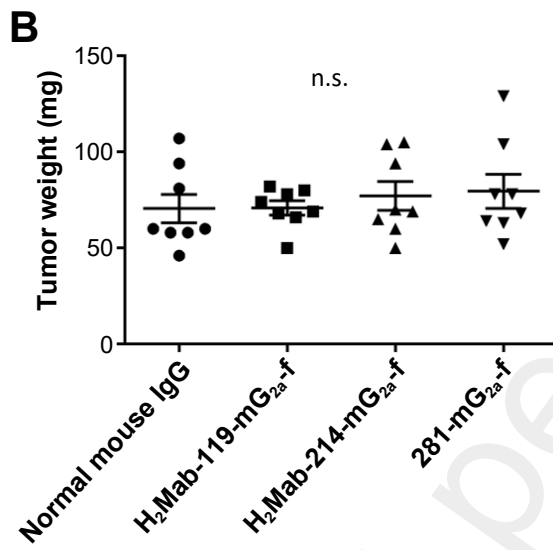
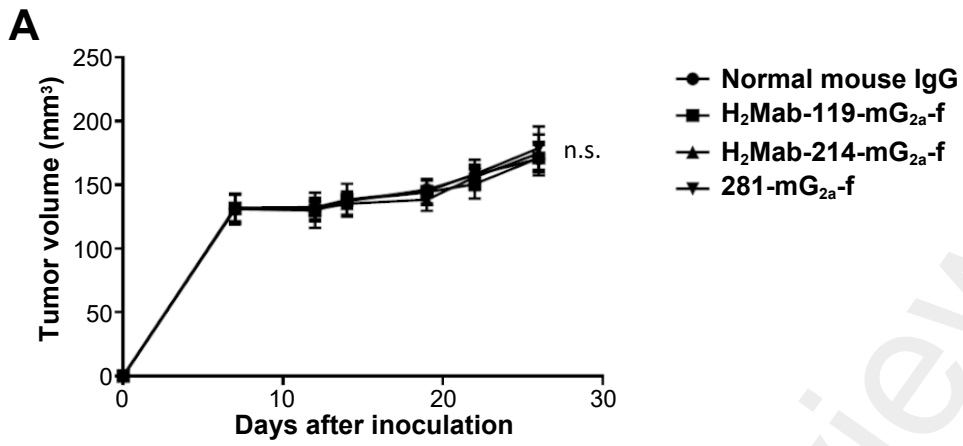


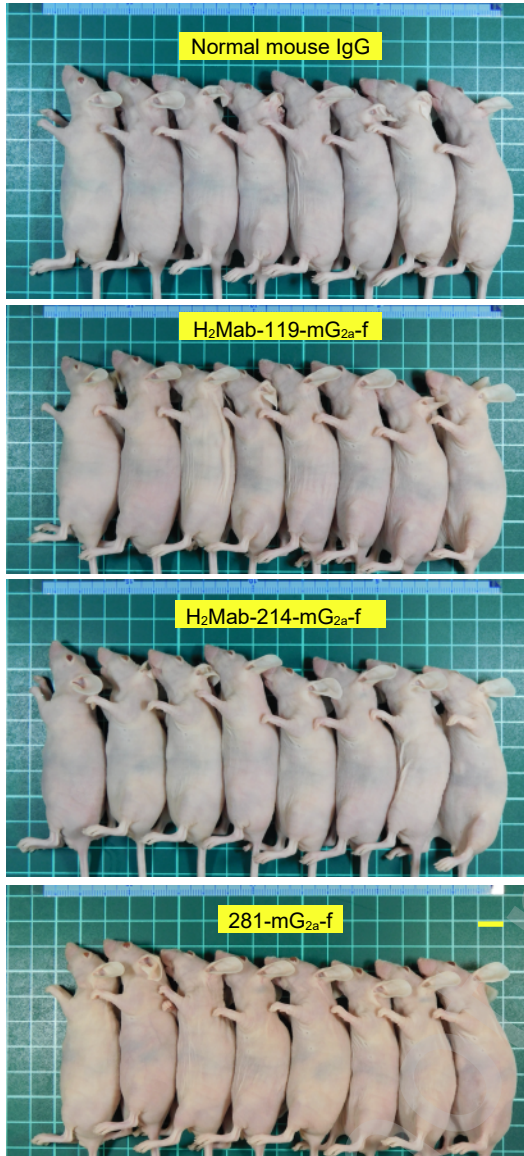
**D**

23 TQVCTGTDMLRLPASPE~~TH~~LDMLRHLYQGCQVVQGNLELTYLPTNASLSFLQDI  
 QEVQGYVLI~~AHNQVRQVPLQRLRIVRGTQLF~~~~EDNY~~ALAVLDNGDPLNNTTPVTGA  
 SPGGLRELQRL~~SLTEILKGGVLIQRNPQLCYQDTILWKDIFHKNNQLALTL~~IDTN  
 RSRACHPCSPMCKGSR~~CWG~~ESSEDCQSLT 216







**A****B**